

See discussions, stats, and author profiles for this publication at: <https://www.researchgate.net/publication/349927263>

# Cranial Anatomy and Dentition of the Aetosaur *Typhothorax Coccinarum* (Archosauria: Pseudosuchia) from the Upper Triassic (Revueltian–Mid Norian) Chinle Formation of Arizona

Article in *Journal of Vertebrate Paleontology* · March 2021

DOI: 10.1080/02724634.2020.1876080

CITATION

1

READS

109

3 authors:



**William A Reyes**

University of Texas at Austin

5 PUBLICATIONS 1 CITATION

[SEE PROFILE](#)



**William G Parker**

National Park Service

170 PUBLICATIONS 2,300 CITATIONS

[SEE PROFILE](#)



**Adam D Marsh**

National Park Service

94 PUBLICATIONS 167 CITATIONS

[SEE PROFILE](#)

Some of the authors of this publication are also working on these related projects:



Cranial description of an aetosaur from the Late Triassic Chinle Formation [View project](#)



Endocranial Morphology of Late Triassic Pseudosuchians [View project](#)





## Cranial Anatomy and Dentition of the Aetosaur *Typothorax Coccinarum* (Archosauria: Pseudosuchia) from the Upper Triassic (Revueltian–Mid Norian) Chinle Formation of Arizona

William A. Reyes, William G. Parker & Adam D. Marsh

To cite this article: William A. Reyes, William G. Parker & Adam D. Marsh (2021): Cranial Anatomy and Dentition of the Aetosaur *Typothorax Coccinarum* (Archosauria: Pseudosuchia) from the Upper Triassic (Revueltian–Mid Norian) Chinle Formation of Arizona, Journal of Vertebrate Paleontology, DOI: [10.1080/02724634.2020.1876080](https://doi.org/10.1080/02724634.2020.1876080)

To link to this article: <https://doi.org/10.1080/02724634.2020.1876080>

 View supplementary material 

 Published online: 09 Mar 2021.

 Submit your article to this journal 

 View related articles 

 View Crossmark data 



# CRANIAL ANATOMY AND DENTITION OF THE AETOSAUR *TYPOTHORAX COCCINARUM* (ARCHOSAURIA: PSEUDOSUCHIA) FROM THE UPPER TRIASSIC (REVUELTIAN–MID NORIAN) CHINLE FORMATION OF ARIZONA

WILLIAM A. REYES, <sup>1,2\*</sup> WILLIAM G. PARKER, <sup>1</sup> and ADAM D. MARSH <sup>1</sup>

<sup>1</sup>Division of Resource Management, Petrified Forest National Park, Petrified Forest, Arizona 86028 U.S.A., [william\\_parker@nps.gov](mailto:william_parker@nps.gov), [adam\\_marsh@nps.gov](mailto:adam_marsh@nps.gov);

<sup>2</sup>Jackson School of Geosciences, University of Texas at Austin, Austin, Texas 78712 U.S.A., [Will\\_Reyes@utexas.edu](mailto:Will_Reyes@utexas.edu)

**ABSTRACT**—Our understanding of *Typhorax coccinarum* is primarily based on postcranial material, along with a few isolated cranial elements. Here we describe the first complete articulated skull of *Typhorax coccinarum* from the Owl Rock Member of the Late Triassic Chinle Formation in Petrified Forest National Park. We assessed the relationships and defining synapomorphies for some of the major clades within Aetosauria by using a combination of morphological characters in the cranium of *Typhorax coccinarum*. Based on the descriptions of skulls from a variety of aetosaur species including *Aetosaurus ferratus*, *Aetosauroides scagliai*, *Coahomasuchus chathamensis*, *Neoetosauroides engaeus*, *Paratyphorax andressorum*, *Stagonolepis olenkae*, *Stenomyti huangae*, *Scutarx deltatylus*, and now *Typhorax coccinarum*, it is apparent that the two major aetosaurian clades vary in their overall skull morphologies. The stagonolepidoids share a more robust, elongate skull, with varying degrees in the lateral expansion of the premaxillary tips. On the other hand, aetosaurines share an overall shorter, more gracile skull with tapered premaxillae. These new characters are mapped onto a revised phylogenetic tree for the Aetosauria. Historically, aetosaurs were interpreted as being predominantly herbivorous. In recent years, the discovery of new aetosaur cranial material, like that of *Neoetosauroides engaeus* and *Aetosauroides scagliai*, suggested an omnivorous diet for at least some aetosaur taxa. The dentition of *Typhorax coccinarum* possesses the most strongly developed heterodonty for an aetosaur, therefore challenging the historical interpretation by expanding the range of dentition types within Aetosauria. This supports the more recent hypothesis that aetosaurs exhibited diverse feeding strategies beyond just herbivory.

**SUPPLEMENTAL DATA**—Supplemental materials are available for this article for free at [www.tandfonline.com/UJVP](http://www.tandfonline.com/UJVP)

Citation for this article: Reyes, W.A., W.G. Parker, and A.D. Marsh. 2021. Cranial anatomy and dentition of the aetosaur *Typhorax coccinarum* (Archosauria: Pseudosuchia) from the Upper Triassic (Revueitian–mid Norian) Chinle Formation of Arizona. *Journal of Vertebrate Paleontology*. DOI: 10.1080/02724634.2020.1876080

## INTRODUCTION

Aetosaurs are a group of heavily armored, quadrupedal pseudosuchian archosaurs restricted to Upper Triassic (Carnian–Rhaetic) rocks of Europe, India, Africa, and North and South America (Walker, 1961; Heckert and Lucas, 2000; Desojo et al., 2013). Most of our understanding about aetosaurs is predominantly based on postcranial elements that include osteoderms, pelvic bones, and vertebrae (Long and Murry, 1995; Desojo et al., 2013; Parker, 2016a). Aetosaur osteoderms (including fragments) are amongst the most abundant fossils from global Upper Triassic strata (Heckert and Lucas, 2000). Aetosaur cranial material is rare, but a few complete or mostly complete skulls have been described in the last decade including those of *Aetosauroides scagliai* (Biacchi Brust et al., 2018), *Scutarx deltatylus* (Parker, 2016a, 2016b), *Paratyphorax andressorum* (Schoch and Desojo, 2016), *Stenomyti huangae* (Small and

Martz, 2013), *Coahomasuchus chathamensis* (Heckert et al., 2017), and *Stagonolepis olenkae* (Sulej, 2010).

Thanks to the discovery of this new skull material, it has become possible to understand the variation in cranial morphology within Aetosauria. Aetosaurs are characterized by their specialized skulls with partially edentulous mandibles, an anteriorly-upturned premaxilla, and laterally facing supratemporal fenestrae (Walker, 1961; Desojo et al., 2013). Originally, the general consensus was that aetosaurs were primarily herbivorous (Walker, 1961; Parrish, 1994; Heckert and Lucas, 2000). However, with the recent discovery of dentigerous material from *Desmatosuchus smalli* (Small, 2002; Parker, 2005a), *Stagonolepis olenkae* (Sulej, 2010), *Stenomyti huangae* (Small and Martz, 2013), and *Aetosauroides scagliai* (Biacchi Brust et al., 2018) it is hypothesized that their diets range between being herbivorous, omnivorous, and carnivorous (Small, 2002; Desojo and Vizcaíno, 2009; Desojo et al., 2013). This range in diet shows just how ecologically adaptive aetosaurs were during the Late Triassic as local and regional environmental conditions fluctuated (Dubiel et al., 1991; Kent and Tauxe, 2005; Nordt et al., 2015).

The majority of known species are recorded from North American terrestrial assemblages (Long and Murry, 1995; Heckert and Lucas, 2000). Most vertebrate assemblages containing aetosaurs known from North America are collected from the Upper Triassic Chinle Formation (Long and Murry, 1995; Heckert and Lucas,

\*Corresponding author.

The work of William A. Reyes, William G. Parker and Adam D. Marsh was authored as part of their official duties as Employees of the United States Government and is therefore a work of the United States Government. In accordance with 17 USC. 105, no copyright protection is available for such works under US Law.

Color versions of one or more of the figures in the article can be found online at [www.tandfonline.com/ujvp](http://www.tandfonline.com/ujvp).

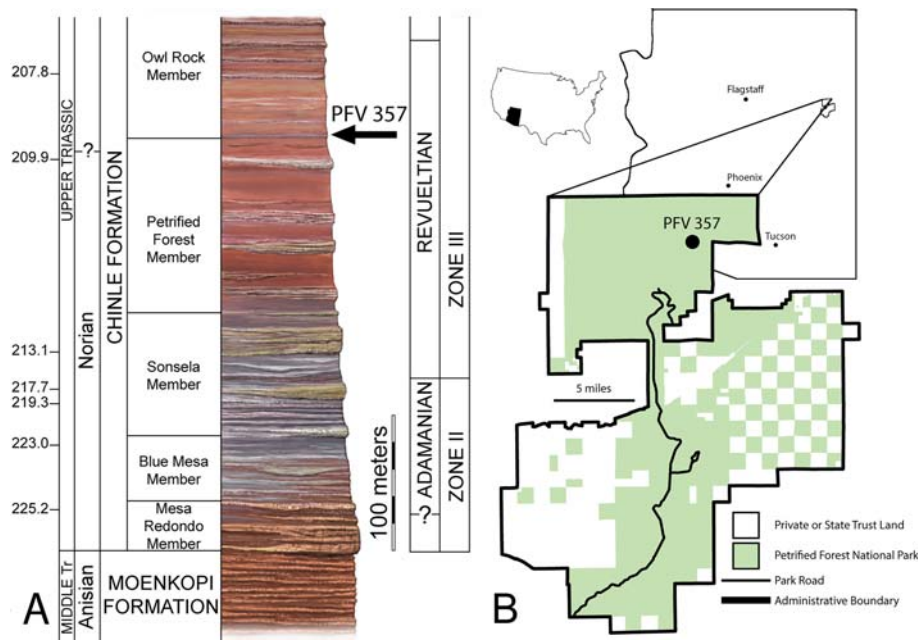


FIGURE 1. Stratigraphic and geographic occurrence of PEFO 38001 in the Late Triassic Chinle Formation within Petrified Forest National Park. **A**, Composite stratigraphic section on the Chinle Formation at Petrified Forest showing the locality in the base of the Owl Rock Member; **B**, Location of PFV 357 within the park boundary in Arizona, U.S.A. Ages from Kent et al., 2018, 2019. **Abbreviations:** Tr, Triassic. Scale bars equal 100 meters and 5 miles, respectively.

2000), particularly from outcrops located within Petrified Forest National Park (PEFO), Arizona (Long and Ballev, 1985; Long and Murry, 1995; Parker, 2005b; Parker and Martz, 2011). Aside from phytosaur teeth, aetosaur osteoderms are the most commonly recovered vertebrate fossils within PEFO, and they are found in strata with ages throughout the Norian (Irmis et al., 2011; Ramezani et al., 2011; Kent et al., 2018). Paleontological investigations in the park in 2008 by a crew from the Yale Peabody Museum resulted in the discovery of two articulated *Typhothorax coccinarum* partial skeletons (PEFO 38001; also catalogued as YPM VP.58121; Fig. 1), one of which has been partially prepared. Until recently the best available materials of *Typhothorax coccinarum* included AMNH 2713 (Cope, 1887; Von Huene, 1915; Parker, 2013), associated material, including partially articulated tail segments, from the Canjilon Quarry in New Mexico (UCMP locality V2816; Nesbitt and Stocker, 2008; Long and Murry, 1995:figs. 100, 105–112), and a variety of postcrania from the Post Quarry in Texas (Martz, 2002; Martz et al., 2013). Heckert et al. (2010) provided the first descriptions of two relatively complete articulated skeletons (NMMNH P-56299, Heckert et al., 2010:figs. 2–5; NMMNH P-12964, Heckert et al., 2010:figs. 6–8) of *Typhothorax coccinarum*. Although the skull material of NMMNH P-12964 can only be studied from a cast, both of these specimens allowed for a complete reconstruction of *Typhothorax coccinarum* (Heckert et al., 2010:fig. 9).

One of the articulated *Typhothorax coccinarum* skeletons (PEFO 38001) found at PEFO includes a complete articulated skull. Aside from the cranial material of NMMNH P-12964 in Heckert et al. (2010:figs. 6–8), the only other cranial material of *Typhothorax coccinarum* (TTU-P 9214) was described by Martz (2002:figs. 4.2, 4.3), which included an isolated dentary and braincase; however, Heckert et al. (2010) suggested this material could pertain to a different taxon. Hence, we aim to provide a comparative description of the cranial morphology of *Typhothorax coccinarum* (PEFO 38001), with the goal of understanding the interspecific variation in cranial anatomy among aetosaurs and what it can tell us about their ecological adaptations.

**Institutional Abbreviations**—AMNH, American Museum of Natural History, New York, New York, U.S.A.; DMNH, Denver Museum of Nature and Science, Denver, Colorado, U.S.A.; PEFO, Petrified Forest National Park, Arizona, U.S.A.

(PFV refers to a locality number from PEFO); NMMNH, New Mexico Museum of Natural History and Science, Albuquerque, New Mexico, U.S.A.; SMNS, Staatliches Museum für Naturkunde, Stuttgart, Germany; TTU-P, Museum of Texas Tech University, Lubbock, Texas, U.S.A.; UCMP, University of California Museum of Paleontology, Berkeley, California, U.S.A.; USNM, Smithsonian National Museum of Natural History, Washington D.C., U.S.A.; UFSM, Universidade Federal de Santa Maria, Santa Maria, Brazil; YPM, Yale Peabody Museum of Natural History, New Haven, Connecticut, U.S.A.

**Materials and Methods**—The skull of PEFO 38001 was prepared by preparators at both the YPM and PEFO. The lateral surfaces of the skull were stabilized with thin Paraloid B-72; a combination of Paraloid B-72 with ground matrix was used as a structural fill to stabilize the skull where needed. The snout was heavily eroded, so a combination of glass microbeads and thin Paraloid B-72 was used to support the fragile bones. The skull was stabilized with cyclododecane during transport from YPM. The skull of PEFO 38001 was CT-scanned at the Summit Healthcare Medical Center in Show Low, Arizona; it was scanned at a beam energy of 1.25kV resulting in 399 slices, with a slice thickness of 140  $\mu\text{m}$ , and a space of 500  $\mu\text{m}$  in between slices. Analysis of the images and 3D reconstructions were developed with the open source software 3D-Slicer v4.10.2 (Fedorov et al., 2012).

#### SYSTEMATIC PALEONTOLOGY

ARCHOSAURIA Cope 1869, sensu Gauthier and Padian, 1985

PSEUDOSUCHIA Zittel 1887–1890, sensu Gauthier and Padian, 1985

AETOSAURIA Marsh 1884, sensu Parker 2007

TYPOTHORACINAE von Huene 1915, sensu Parker 2016a

*TYPOTHORAX* Cope 1875

*TYPOTHORAX COCCINARUM* Cope 1875

Figs. 2–7

**Holotype Specimen**—USNM 2585, five osteoderm fragments (Cope 1875; see discussion in Parker, 2013).

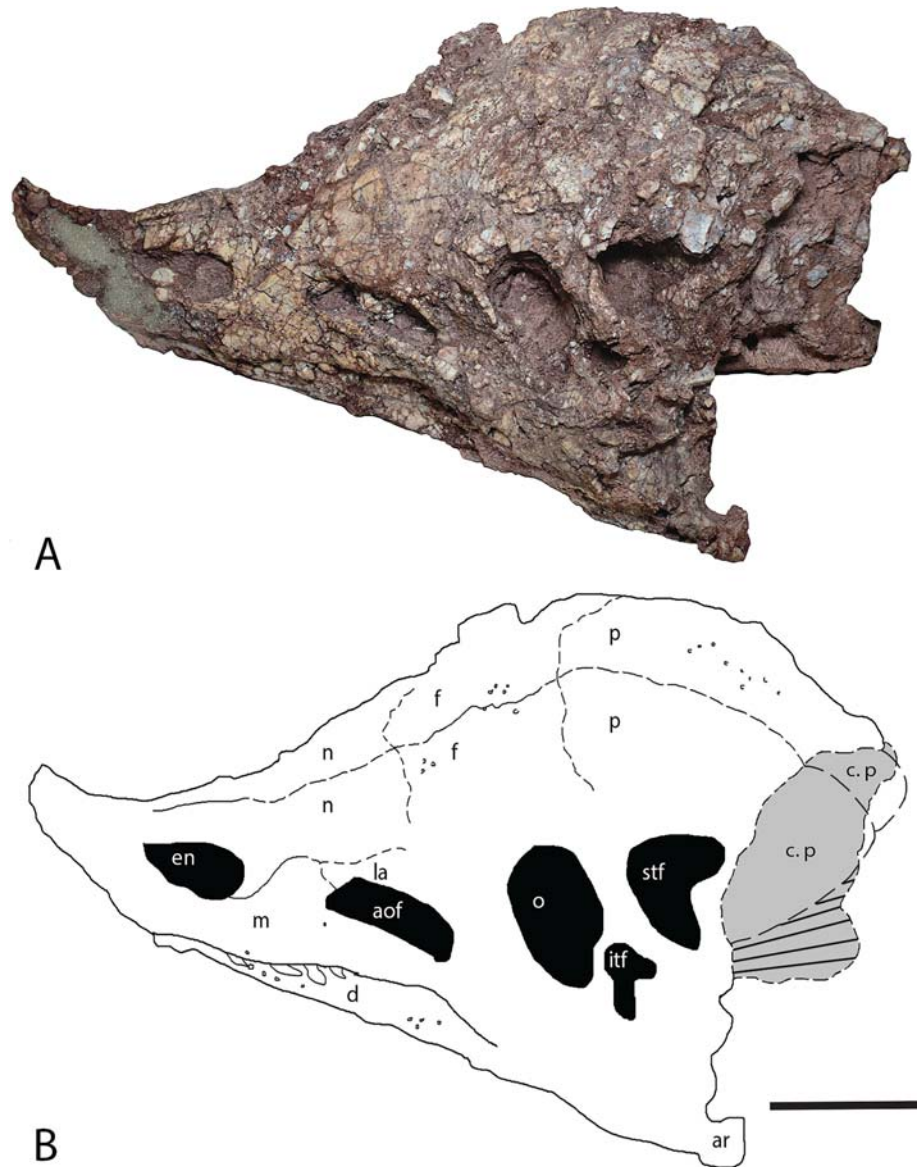


FIGURE 2. **A**, PEFO 38001 in left lateral view; **B**, Interpretive sketch with bone elements and fossa outlined. **Abbreviations:** aof, antorbital fenestra; ar, articular; c.p, assumed cervical paramedian articulation to cranium; d, dentary; en, external naris; f, frontal; itf, infra-temporal fenestra; la, lacrimal; m, maxilla; n, nasal; o, orbit; p, parietal; stf, supratemporal fenestra. Scale bar equals 5 cm.

**Referred Specimen**—PEFO 38001/YPM VP.58121, temporarily refers to two overlapping, semi-articulated, and incomplete skeletons of *Typhothorax coccinarum* from the Late Triassic Chinle Formation, Petrified Forest National Park. The associated postcrania (primarily the osteoderms) of both skeletons allows for the identification of the taxon. The temporary catalog number is due to the overlap between the disarticulated segments of the two skeletons. At this point it is difficult to determine which disarticulated bones belong to which skeleton without further preparation. The referred skull is temporarily located at PEFO and will be sent on a long-term loan to the YPM where the rest of PEFO 38001 is being prepared.

**Geological Setting**—PFV 357 (YPM UT-AZ-08-36, Patio Quarry); ‘purple gray bed,’ a well-calcified bed at the base of the Owl Rock Member (Fig. 1), Chinle Formation, ~209 Ma (sensu Dubiel, 1989; Martz et al., 2012; Kent et al., 2019), Revueltian land vertebrate estimated holochronozone (Martz and Parker, 2017). Within PEFO the Owl Rock

Member is a heterolithic interval of sandstone and mudstone with minor siltstone and limestone (Martz et al., 2012); exposed primarily at Chinde Mesa (upper part of the Owl Rock Member) and Pilot Rock (‘purple gray bed’ and lower part of the Owl Rock Member), along the northern boundary of PEFO (Martz et al., 2012). Not many vertebrates have been collected from the Owl Rock Member at PEFO, and the majority are locally from the ‘purple gray bed’ (Martz et al., 2012). Previously, fragments of *Typhothorax coccinarum* (PEFO 34929) were collected just above the Black Forest bed within the Petrified Forest Member making it the highest known occurrence of this taxon within PEFO (Parker, 2016a); the discovery of PEFO 38001 expands the biostratigraphical range of *Typhothorax coccinarum* to the base of the Owl Rock Member within the park, although this taxon has been documented from the Owl Rock Member elsewhere in northern Arizona (Kirby, 1991, 1993; Spielmann et al., 2007; Parker and Martz, 2011).

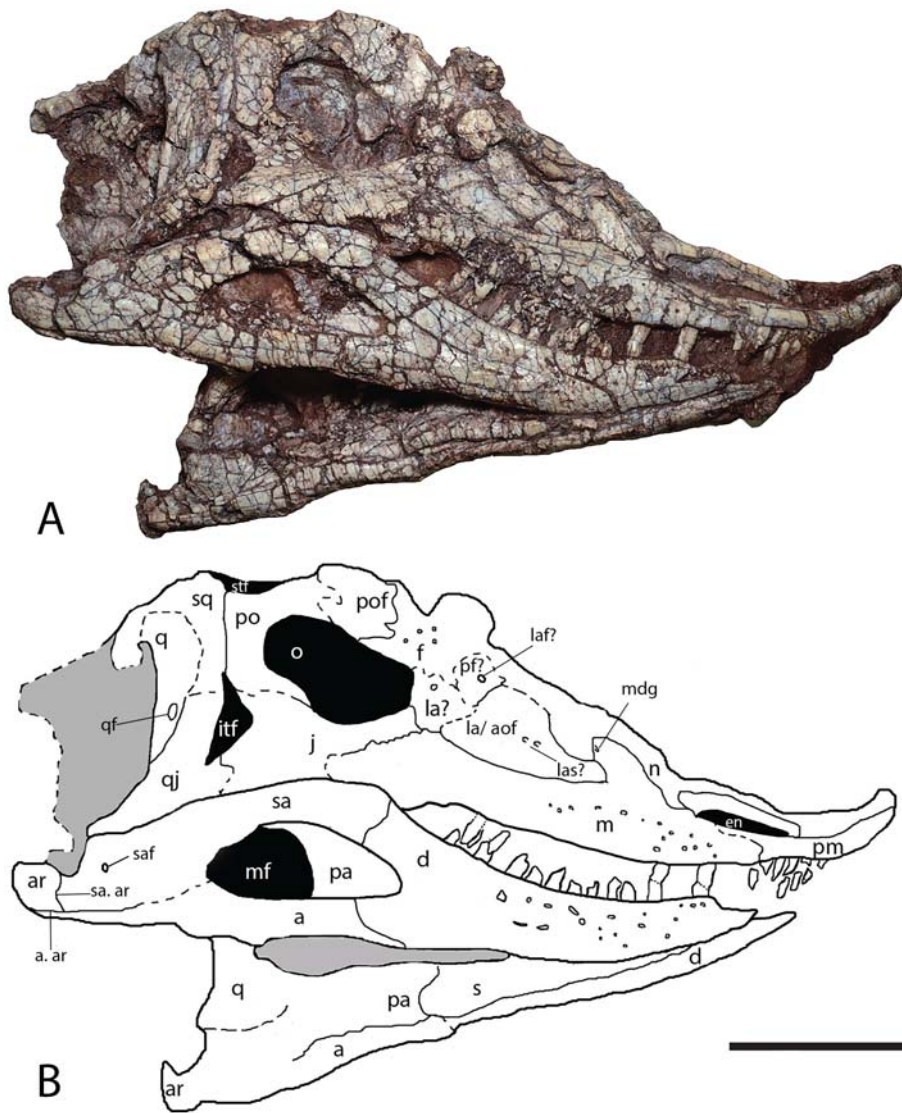


FIGURE 3. **A**, PEFO 38001 in right lateral view; **B**, Interpretive sketch with bone elements and fossa outlined. **Abbreviations:** **a**, angular; **a. ar**, angular-articular contact; **aof**, antorbital fenestra; **ar**, articular; **d**, dentary; **en**, external naris; **f**, frontal; **itf**, infratemporal fenestra; **j**, jugal; **la**, lacrimal; **laf**, lacrimal foramen; **las?**, lacrimal sculpturing; **m**, maxilla; **mdg**, maxillary dorsal groove; **mf**, mandibular fenestra; **n**, nasal; **o**, orbit; **pa**, prearticular; **pf**, prefrontal; **pm**, premaxilla; **po**, postorbital; **pof**, postfrontal; **q**, quadrate; **qf**, quadrate foramen; **qj**, quadratojugal; **s**, splenial; **sa**, surangular; **saf**, surangular foramen; **sa. ar**, surangular-articular contact; **sq**, squamosal; **stf**, supratemporal fenestra. Scale bar equals 5 cm.

## CRANIAL DESCRIPTION

The skull is mediolaterally compressed such that the dorsal and left lateral surfaces of the skull are displaced anteroventrally, and the right lateral surface remains mostly unaltered. Because of this deformation, the skull has a posterior width of ~2.5 cm (prior to displacement the width would be ~9 cm), maximum anteroposterior length of ~21 cm, and a maximum dorsoventral height of ~13 cm. The outer surface of the skull is significantly weathered, particularly the left side (Fig. 2A). Many of the individual bones are difficult to interpret because of this weathering. The midline sutures between the nasal and frontal bones are visible. Many of the teeth are crushed and broken (Fig. 3A), but the few teeth present are preserved well enough for a detailed description of their shape and texture. There appear to be five premaxillary teeth preserved on the right premaxilla, a total of eight preserved maxillary teeth with four on each maxilla, and nine teeth on the right dentary. The flattening of the skull does not allow for a description of the palatal complex in this specimen of *Typosuchus coccinarum*.

## Cranium

This description is predominantly based on the right half of the skull (Fig. 3). The anteroposterior length of the cranium is ~21 cm and has a maximum dorsoventral height of ~6 cm (right lateral) and ~12 cm (left lateral) from the ventral base of the jugal to the dorsal margin of the frontal; prior to deformation the cranium would have been ~9 cm dorsoventrally. The fenestrae of the left side of the skull (Fig. 2) are distorted and the anterior half of the external naris is eroded, so only measurements of the fenestrae on the right side were taken.

The external naris is elliptical with an anteroposterior length of ~3.5 cm and a maximum height of ~1 cm. This is a common proportion in aetosaurs, as seen in *Aetosauroides scagliai* (Biacchi Brust et al., 2018), *Neo-aetosauroides engaeus* (Desojo and Báez, 2007), and *Paratyposuchus andressorum* (SMNS 19003; Schoch and Desojo, 2016). The medial surface of the nasal forms the dorsal half of the narial opening. The external naris is ~17% the length of the cranium, which is a low percentage compared with that of *Desmotosuchus smalli* (Small, 2002) and *Stagonolepis robertsoni* (Walker, 1961), in which the external

naris is ~25% the length of the cranium. The antorbital fenestra is also elliptical with an anteroposterior length of 4.1 cm and a maximum height of 2.2 cm near the posterior end, similar in shape to that of *Paratyphothorax andressorum* (Schoch and Desojo, 2016:fig. 3b). The crushed lacrimal is visible through the fenestra. The orbit is distorted anterodorsally and slightly narrows posterodorsally into a more circular margin as it contacts parts of the postorbital, postfrontal, and frontal bones posterodorsally. The orbit is bordered by the lacrimal (anteriorly), frontal and postfrontal (dorsally), postorbital (posteriorly), jugal (ventrally), and has an anteroposterior length of ~3.8 cm with a maximum dorsoventral height of 3.1 cm near its center; because of the compression of the skull, the laterosphenoid is pressed laterally into the orbit. The infratemporal fenestra is shaped like an obtuse triangle with an anteroposterior length of 0.7 cm and a dorsoventral height of 1.8 cm, similar to that of *Stagonolepis robertsoni* (Walker, 1961), *Paratyphothorax andressorum* (Schoch and Desojo, 2016), *Coahomasuchus chathamensis* (Heckert et al., 2017), and *Neoaetosauroides engaeus* (Desojo and Báez, 2007); unlike that of *Aetosaurus ferratus* (Schoch, 2007), which is bean-shaped. The supratemporal fenestra is poorly preserved on both sides of the skull; the right supratemporal fenestra is obscured by crushed bone fragments (Fig. 3), and the left fenestra has been distorted and is posteriorly eroded (Fig. 2). The supratemporal fenestra would have been broadly ellipsoidal in shape, with an anteroposterior length of 2.3 cm and a dorsoventral height of 2.9 cm.

**Premaxilla**—The premaxilla is an elongate, slender bone with an anteroposterior length of ~6 cm and a dorsoventral height of ~5 mm (Fig. 3). The premaxilla makes up most of the ventral margin of the external naris. The anterior end of the premaxilla upturns dorsally about 20–35° from the horizontal into an elongated tip, which appears to be apomorphic for *Typhothorax coccinarum*. This elongated tip is also visible in an articulated skeleton of *Typhothorax coccinarum* (NMMNH P-12964; Heckert et al., 2010:fig. 8a–c). The distal ends of the premaxillae in PEFO 38001 lack the lateral expansion forming the ‘shovel-tipped’ snout found in several aetosaurian taxa, particularly in the stagonolepidoid aetosaurus which includes *Desmatosuchus smalli* (Small, 2002), *Stagonolepis robertsoni* (Walker, 1961), *Stagonolepis olenkae* (Sulej, 2010), and *Neoaetosauroides engaeus* (Desojo and Báez, 2007; Desojo et al., 2013). The laterally expanded tip is also lacking in other aetosaurine aetosaurus; this includes *Aetosaurus ferratus* (Schoch, 2007), *Paratyphothorax andressorum* (Schoch and Desojo, 2016), and *Stenomyti huangae* (Small and Martz, 2013), where the premaxillae form a laterally narrow edentulous tip, but do not strongly recurve upwards as in *Typhothorax coccinarum*. Heckert et al. (2010:fig. 8a–c) figured a skull of *Typhothorax coccinarum* (NMMNH P-12964) that also shows the premaxilla curving dorsally, but the skull of NMMNH P-12964 has not been described in detail for comparison. In PEFO 38001 the anterior half (~2 cm) of the premaxilla is edentulous, while the posterior half appears to bear five teeth (Fig. 3B). Posteriorly, a thin projection that borders the posteroventral portion of the external naris extends ~2 cm overlapping the anterior portion of the maxilla. The suture with the nasal is not discernible.

**Maxilla**—The maxilla of PEFO 38001 is triradiate, main body and three processes, in lateral view and is exposed well on both sides of the skull (Figs. 2, 3). Laterally, it has an anteroposterior length of 8.5 cm. The anterior ramus has a maximum dorsoventral height of 1.2 cm and a wedge-shaped contact with the premaxilla, similar to that of *Desmatosuchus smalli* (Small, 2002) and *Stenomyti huangae* (Small and Martz, 2013). Anterodorsally, the maxilla is slightly involved in the posteroventral margin of the external naris (Figs. 2, 3). The posterior ramus is the largest branch of the maxilla; anteroposteriorly the length of the ramus is 5.5 cm, and has a maximum dorsoventral height of 1.5

cm. Additionally, the posterior ramus has a curved overlapping contact with the jugal forming the entire ventral margin of the antorbital fenestra. The ascending dorsal process has an anteroposterior length of 1.3 cm, forms the anterior margin of the antorbital fenestra, and has a long, curved contact with the ventral edge of the nasal and also contacts the lacrimal posterodorsally. On the dorsal ramus (Fig. 3B), there is a small groove that is part of the suture with the nasal.

A row of nutrient foramina is present on the lateral surface of the maxilla, and they are concentrated near the ventral margin just above the teeth, a condition also seen in *Desmatosuchus smalli* (Small, 2002). The ventral margin of the maxilla is gently curved like in *Stagonolepis olenkae* (Sulej, 2010:fig. 9e), not straight like in *Neoaetosauroides engaeus* (Desojo and Báez, 2007:fig. 5). Weathered sculpturing is visible above the row of nutrient foramina. It is interpreted that the foramina extend anteroposteriorly from the contact with the premaxilla up to the most posterior tooth, because there are signs of crushed foramina on bone fragments towards the posterior half of the posterior ramus of the maxilla; the foramina extend to the most posterior maxillary tooth in *Longosuchus meadei* (Parrish, 1994), *Aetosaurus ferratus* (Schoch, 2007), and both *Stagonolepis* species (*S. robertsoni* and *S. olenkae*; Walker, 1961; Sulej, 2010). These foramina transmitted fibers of the maxillary branch of the trigeminal nerve (CN V<sub>2</sub>; George and Holliday, 2013). Based on CT imagery (Fig. 4C) and an isolated, but much larger, maxilla of *Typhothorax coccinarum* (PEFO 42506), the ‘pneumatic accessory cavity’ seen medially on the maxilla of *Desmatosuchus smalli* (Small, 2002:fig. 4), and both *Stagonolepis* species (*S. robertsoni* and *S. olenkae*; Walker, 1961; Sulej, 2010) is not present in *Typhothorax coccinarum*.

Four maxillary teeth are preserved in each maxilla (Figs. 2, 3). An exact tooth count is difficult because most of the teeth near the center of the maxilla on the right lateral side are crushed (Fig. 3), but based on PEFO 42506 it may have included eight alveoli, similar to *Stenomyti huangae* (Small and Martz, 2013), *Aetosaurus ferratus* (Schoch, 2007), and *Neoaetosauroides engaeus* (Desojo and Báez, 2007), which each have eight maxillary teeth. The alveoli in PEFO 38001 are deep (Fig. 4C), which is also a feature seen in the maxilla of PEFO 42506.

**Nasal**—The nasal is the most anteroposteriorly elongate bone of the skull roof with an anteroposterior length of 8.5 cm, or ~40% the length of the cranium. In dorsal view, the nasals have a triangular shape, the midline suture is partially visible (Fig. 2), and they narrow anteriorly into a tip as they contact the premaxillae; this condition is seen in the aetosaurine aetosaurus *Paratyphothorax andressorum* (Schoch and Desojo, 2016), *Stenomyti huangae* (Small and Martz, 2013), *Aetosaurus ferratus* (Schoch, 2007), and *Neoaetosauroides engaeus* (Desojo and Báez, 2007). On the other hand, this condition is not seen in stagonolepidoid aetosaurus (Parker 2016a:fig. 7; Hoffman et al., 2018:fig. 5) like *Desmatosuchus smalli* (Small, 2002), and both *Stagonolepis* species (*S. olenkae* and *S. robertsoni*; Walker, 1961; Sulej, 2010), which have an anterolaterally wide contact with the premaxilla. The nasal is mediolaterally broadest posteriorly (~2 cm), where it contacts the frontal, and it narrows down to ~1 cm halfway above the external naris. Ventrally, the nasal contacts the dorsal margins of the lacrimal, maxilla, and forms the dorsal margin of the external naris. Near the middle of the nasal, there is a projection that extends ventrally and underlies the posterior end of the external naris. This projection is seen in *Aetosauroides scagliai* (Biacchi Brust et al., 2018), *Aetosaurus ferratus* (Schoch, 2007), *Paratyphothorax andressorum* (Schoch and Desojo, 2016), but not in *Desmatosuchus smalli* (Small, 2002). No foramina are present on the lateral surface of the nasal.

**Lacrimal**—The lacrimal is crushed and collapsed into the antorbital fenestra (Fig. 3). The exact shape is not recognizable,

but it can be approximated based on the skulls of *Paratypothorax andressorum* (Schoch and Desojo, 2016) and *Stenomyti huangae* (Small and Martz, 2013); these taxa are close relatives of *Typothorax coccinarum* (Parker, 2016a:fig. 7; Hoffman et al., 2018:fig. 5). The lacrimal has an approximate anteroposterior length of 4.8 cm and dorsoventral height of 1.4 cm near the posterior border. Ventrally, it would form the dorsal margin of the antorbital fenestra. The lacrimal would contact the maxilla anteriorly. Dorsally, it contacts the posteroventral margin of the nasal and possibly the anteroventral margin of the prefrontal, similar to that of *Paratypothorax andressorum* (Schoch and Desojo, 2016). Posteriorly, the lacrimal should contact the prefrontal posterodorsally, the jugal posteroventrally, and be involved in the anterior margin of the orbit. There is radial sculpturing on the lateral surface of the lacrimal.

**Prefrontal**—The shape and sutural contacts of the prefrontal are unrecognizable on this specimen of *Typothorax coccinarum* (PEFO 38001). It might be represented by a raised fragment of bone containing a foramen (Fig. 3B) on the posterodorsal margin of the collapsed lacrimal. This block of bone could also be part of the lacrimal with the lacrimal foramen exposed on the lateral surface. It is not possible to compare the prefrontal of PEFO 38001 to that of other aetosaurs because of its crushed state (Fig. 3).

**Frontal**—Because of the distortion both frontal bones and their midline sutures are visible on the left side of the specimen (Fig. 2). The frontal is anteroposteriorly shorter than the nasal with a length of 3.5 cm (~41% the anteroposterior length of the nasal), but is mediolaterally wider with a width of ~3 cm. There is a radial sculpturing texture on the lateral surface of the frontal, unlike the nasal; *Scutaxx deltatylus* (Parker, 2016b:fig. 5) also exhibits this sculpturing texture on the frontal. This aids in distinguishing the anterior contact of the frontal with the nasal. Ventrally, the frontal forms part of the anterodorsal margin of the orbit and may contact either the prefrontal or lacrimal. Posteriorly, it contacts the anterior margins of the parietal and postfrontal.

**Parietal**—Like the frontals, both of the parietal bones are visible on the left side of the specimen (Fig. 2) but they are severely weathered; the surface of the bone is crushed into small fragments, and the posterior ends are partially eroded. The parietal forms the posterodorsal surface of the skull roof. Just like the frontal, the parietal has a radial sculpturing texture on the lateral surface. The parietal has an anteroposterior length of ~6 cm and a mediolateral width of 2.5 cm. The parietal contacts the frontal anteriorly. Ventrally, the parietal forms the dorsal margin of the supratemporal fenestra. Posteriorly, there are signs of a reminiscent transverse crest where the first set of cervical paramedian osteoderms would overlap (Fig. 2B). This is a condition also seen in *Desmatosuchus smalli* (Small, 2002), *Stenomyti huangae* (Small and Martz, 2013), *Neoaetosauroides engaeus* (Desojo and Báez, 2007), *Aetosauroides scagliai* (Biacchi Brust et al., 2018), *Stagonolepis robertsoni* (Walker, 1961), and *Paratypothorax andressorum* (Schoch and Desojo, 2016). Details of the contacts between the parietal and the squamosal, postorbital, frontal, or supraoccipital are not discernible.

**Jugal**—In *Typothorax coccinarum* (PEFO 38001) the jugal is a strongly triradiate bone (Fig. 3), unlike that of *Paratypothorax andressorum* (Schoch and Desojo, 2016:fig. 5), which is more rectangular in shape. The right jugal is oblique dorsolaterally, giving it the impression of a ‘cheek’ (Fig. 3). It is anteroposteriorly longer (4.8 cm, as long as the orbit) than dorsoventrally tall (1.7 cm). Dorsally, the jugal forms the ventral margin of the orbit. The anterior ramus has an anteroventral overlapping contact with the maxilla, an ascending anterodorsal contact with the lacrimal, and forms the anteroventral margin of the orbit. Posteriorly, the jugal makes the curved (dorsoventrally wide) anterior margin of the infratemporal fenestra while contacting the postorbital and quadratojugal. The posterodorsal

ramus is wedge-shaped; it broadly contacts the ventral margin of the postorbital and forms most of the anterodorsal margin (~8 mm) of the infratemporal fenestra and the posteroventral margin of the orbit. Ventrally, the jugal composes part of the posteroventral margin of the cranium. How much the ventral margin of the cranium is composed by the jugal varies within Aetosauria (Desojo et al., 2013:fig. 4; Schoch and Desojo, 2016:fig. 7); the jugal in *Neoaetosauroides engaeus* (Desojo and Báez, 2007), *Stenomyti huangae* (Small and Martz, 2013), and *Desmatosuchus smalli* (Small, 2002) makes up most (if not all) of the posterior ventral margin of the cranium, while in *Paratypothorax andressorum* (Schoch and Desojo, 2016) and *Aetosaurus ferratus* (Schoch, 2007) the jugal is anteroposteriorly smaller with shorter ventral margins. This margin is not straight like that of *Paratypothorax andressorum* (Schoch and Desojo, 2016), *Coahomasuchus chathamensis* (Heckert et al., 2017), and *Aetosauroides scagliai* (Biacchi Brust et al., 2018). The jugal descends ventrally (Fig. 3) but unlike that of *Longosuchus meadei* (Parrish, 1994), *Desmatosuchus smalli* (Small, 2002), and *Stagonolepis robertsoni* (Walker, 1961), which are characterized by a strongly downturned ventral margin; the jugal is gently downturned posteriorly, less than that of *Neoaetosauroides engaeus* (Desojo and Báez, 2007). The ventral ramus forms most of the anteroventral margin (~1 cm) of the infratemporal fenestra and slightly contacts part of the anterodorsal border of the quadratojugal.

**Quadratojugal**—In PEFO 38001 the quadratojugal is roughly L-shaped and is composed of two main rami: anterior ramus and dorsal ramus (Fig. 3). The anterior ramus seems to have a broad dorsoventral contact with the posteroventral ramus of the jugal, but only ~2 mm of the contact is preserved. Additionally, the anterior ramus makes up the most ventral section (~3 mm) of the anteroventral margin of the infratemporal fenestra. Dorsally, the quadratojugal contacts the ventral ramus of the squamosal. The dorsal contact is anteroposteriorly straight like that of *Neoaetosauroides engaeus* (Desojo and Báez, 2007) and *Desmatosuchus smalli* (Small, 2002), but not as broad; it does not ascend posterodorsally as in *Stagonolepis robertsoni* (Walker, 1961) or *Aetosaurus ferratus* (Schoch, 2007).

The quadratojugal forms most (~1 cm) of the dorsoventrally straight posterior margin of the infratemporal fenestra. Posteriorly, the quadratojugal has a curved contact with the quadrate. Additionally, it tapers posteroventrally similar to that of *Stenomyti huangae* (Small and Martz, 2013) and *Neoaetosauroides engaeus* (Desojo and Báez, 2007). The ventral margin of the quadratojugal posteriorly curves downward, a condition also seen in *Paratypothorax andressorum* (Schoch and Desojo, 2016) and *Stagonolepis robertsoni* (Walker, 1961), but unlike that of *Aetosaurus ferratus* (Schoch, 2007), which curves upwards posteriorly. Although part of the ventral border is eroded, the quadratojugal forms the last ~3 cm of the posteroventral margin of the cranium. Overall, the shape of the quadratojugal varies within Aetosauria; it is roughly L-shaped to some degree (Schoch and Desojo, 2016:fig. 7) but this shape is not seen in *Desmatosuchus smalli* (Small, 2002) and *Paratypothorax andressorum* (Schoch and Desojo, 2016), which lack the anterior ramus that gives it the L-shape.

**Quadrate**—The quadrate is mediolaterally crushed and does not allow for any contacts to be described at the posterior of the skull. It has an anteroposterior width of 1.4 cm and a dorsoventral height of 4.8 cm. Laterally, the height of the quadrate varies within Aetosauria (Desojo et al., 2013:fig. 4); this seems to be dependent on how convex the anterior margin is (i.e., the concavity of the posterior margin shared by the articulated squamosal and quadratojugal). The quadrate of PEFO 38001 does not extend past the ventral margin of the quadratojugal, unlike that of *Stenomyti huangae* (Small and Martz, 2013) and *Paratypothorax andressorum* (Schoch and Desojo, 2016:fig. 4). Dorsally, the head of the quadrate meets with the posteroventral



border of the squamosal (Fig. 3) just underneath the squamosal-horn, a condition seen in other aetosaurs such as *Stenomyti huangae* (Small and Martz, 2013), *Neoaetosauroides engaeus* (Desojo and Báez, 2007), *Coahomasuchus chathamensis* (Heckert et al., 2017), *Desmatosuchus smalli* (Small, 2002), *Paratytophorax andressorum* (Schoch and Desojo, 2016), and both *Stagonolepis* species (*S. robertsoni* and *S. olenkae*; Walker, 1961; Sulej, 2010).

The quadrate foramen probably occurs between the quadrate and quadratojugal like that of *Stenomyti huangae* (Small and Martz, 2013) and *Desmatosuchus smalli* (Small, 2002), but it is not possible to confirm due to its weathered condition. Posteriorly, the quadrate has a concave margin in lateral view (Fig. 3B), a condition also seen in *Stenomyti huangae* (Small and Martz, 2013), *Desmatosuchus smalli* (Small, 2002), *Paratytophorax andressorum* (Schoch and Desojo, 2016), and *Stagonolepis robertsoni* (Walker, 1961); unlike that of *Aetosaurus ferratus* (although slightly concave ventrally; Schoch, 2007:fig. 9a), *Coahomasuchus chathamensis* (Heckert et al., 2017), and *Stagonolepis olenkae* (Sulej, 2010), which have a primarily straight margin. On the left ramus of the mandible (Fig. 3B), the articulation between the quadrate and the mandibular joint is visible medially; this contact appears to be broadly curved anteroposteriorly.

**Postorbital**—Based on PEFO 38001 (Fig. 3B) the postorbital of *Tytophorax coccinarum* is not a well-developed triradiate bone, unlike that of *Stenomyti huangae* (Small and Martz, 2013), *Scutarx deltatylus* (Parker, 2016b), and both *Stagonolepis* species (*S. robertsoni* and *S. olenkae*; Walker, 1961; Sulej, 2010); it lacks the posterior process that broadly overlaps the anterior margin of the squamosal. Hence, the postorbital of *Tytophorax coccinarum* appears more similar to that of *Coahomasuchus chathamensis* (Heckert et al., 2017:fig. 7) and *Aetosaurus ferratus* (Schoch, 2007).

Anteriorly, the postorbital forms the posterior margin of the orbit. The dorsal ramus extends 1.7 cm anteroposteriorly and has a dorsoventral height of ~7 mm. It seems to overlap the posterior border of the postfrontal anteriorly, while ventrally forming part of the posterodorsal margin of the orbit, and dorsally forming the anteroventral margin of the supratemporal fenestra. Posteriorly, the postorbital lacks the posterior process (mentioned above) and has a dorsoventrally straight contact with the squamosal. The ventral ramus extends ~2 cm and has an anteroposterior width of ~8 mm. Ventrally, the postorbital has a tapering anteroventral process that descends and underlies the posteroventral margin of the orbit, a condition also seen in *Stenomyti huangae* (Small and Martz, 2013), *Scutarx deltatylus* (Parker, 2016b), *Paratytophorax andressorum* (Schoch and Desojo, 2016), *Aetosaurus ferratus* (Schoch, 2007), *Neoaetosauroides engaeus* (Desojo and Báez, 2007), and *Coahomasuchus chathamensis* (Heckert et al., 2017); this process receives the posterodorsal ramus of the jugal. Additionally, the ventral ramus participates on the anterodorsal margin of the infratemporal fenestra forming the most dorsal section (~4 mm).

The postorbital of *Tytophorax coccinarum* is separated from the quadratojugal by the descending ventral process of the squamosal, as seen in *Neoaetosauroides engaeus* (Desojo and Báez, 2007), *Stenomyti huangae* (Small and Martz, 2013), *Desmatosuchus smalli* (Small, 2002), *Scutarx deltatylus* (Parker, 2016b), and both *Stagonolepis* species (*S. robertsoni* and *S. olenkae*; Walker, 1961; Sulej, 2010). It is unlike that of *Paratytophorax andressorum* (Schoch and Desojo, 2016), *Aetosaurus ferratus* (Schoch, 2007), and *Coahomasuchus chathamensis* (Heckert et al., 2017) which have a broad posteroventral contact with the anterodorsal border of the quadratojugal; in *Aetosaurus ferratus* (Schoch, 2007) the contact is greatly reduced.

**Postfrontal**—The postfrontal in PEFO 38001 has an antero-posterior length of 1.5 cm and dorsoventral height of 1.7 cm.

It is not heavily ornamented on the lateral surface like in *Paratytophorax andressorum* (Schoch and Desojo, 2016) and *Stagonolepis olenkae* (Sulej, 2010). Posteriorly, the postfrontal appears to overlap the ascending anterior margin of the postorbital; this contact is dorsoventrally broad (Fig. 3B). Ventrally, the postfrontal participates in the dorsal margin of the orbit (Fig. 3). Anteriorly, the suture with the frontal is open, most likely because the elements were displaced as the skull was crushed during burial. The dorsal contact between the postfrontal and parietal is not discernible because the skull has been severely weathered (Figs. 2A, 3A).

Two general features characterize the postfrontal within Aetosauria: (1) the shape of the postfrontal is generally triangular (*Aetosaurus ferratus* being an exception; Schoch, 2007:fig. 8a) and (2) the postfrontal is smaller compared with the prefrontal (Desojo et al., 2013:fig. 4; Biacchi Brust, 2018:fig. 7). These features are seen in most of the described aetosaur skulls that preserve the posterodorsal section of the cranium; examples include *Desmatosuchus smalli* (albeit that no prefrontal has been identified; Small, 2002:fig. 2a), *Paratytophorax andressorum* (Schoch and Desojo, 2016), *Aetosauroides scagliai* (Biacchi Brust, 2018), *Neoaetosauroides engaeus* (Desojo and Báez, 2007), *Aetosaurus ferratus* (Schoch, 2007), *Longosuchus meadei* (Parrish, 1994), *Stenomyti huangae* (Small and Martz, 2013), and both *Stagonolepis* species (*S. robertsoni* and *S. olenkae*; Walker, 1961; Sulej, 2010). The postfrontal of PEFO 38001 has a subrounded square shape, as opposed to it being triangular (Fig. 3). Based on our tentative outlines of the cranial bones (Fig. 3B), the postfrontal is dorsoventrally larger than the prefrontal in *Tytophorax coccinarum*. It is possible that, like *Aetosaurus ferratus* (Schoch, 2007), *Tytophorax coccinarum* does not abide by the general postfrontal features (mentioned above), but it is difficult to confirm solely on the skull of PEFO 38001.

**Squamosal**—The squamosal of PEFO 38001 is mostly unrecognizable because of weathering and crushing. Only the descending ramus and squamosal horn can be identified in lateral view on the right side of the cranium (Fig. 3). Anteriorly, the squamosal has a straight dorsoventral contact with the postorbital. The descending ramus has a dorsoventral height of ~3.2 cm and narrows ventrally to about ~1 cm. Ventrally, it composes the most dorsal section (~4 mm) of the posterodorsal margin of the infratemporal fenestra and separates the quadratojugal from the postorbital. The ventral margin of the descending process of the squamosal is anteroposteriorly curved, as seen in *Neoaetosauroides engaeus* (albeit not as broad; Desojo and Báez, 2007) and *Desmatosuchus smalli* (Small, 2002); it is unlike that of *Aetosaurus ferratus* (Schoch, 2007) and *Stagonolepis olenkae* (Sulej, 2010), which overlap the ventrally descending process of the squamosal with the dorsally ascending process of the quadratojugal.

The squamosal of *Tytophorax coccinarum* has a curved contact with the quadrate unlike that of *Aetosaurus ferratus* (Schoch, 2007:fig. 8a), which has an ascending posterodorsally straight margin. Additionally, it has a well-developed squamosal horn that overhangs the quadrate head (Fig. 3), unlike the less-developed squamosal horns of *Aetosaurus ferratus* (Schoch, 2007) and *Neoaetosauroides engaeus* (Desojo and Báez, 2007); this feature is seen in most aetosaurs, but varies in its prominence between species (Small and Martz, 2013; Desojo et al., 2013:fig. 4). Dorsally, the squamosal forms the posterior margin of the supratemporal fenestra. The occiput contacts of the squamosal with the parietal and paraoccipital process of the opisthotic are not discernible.

## Braincase

Because the skull of PEFO 38001 is mediolaterally compressed neither the occipital bones nor the braincase are readily visible

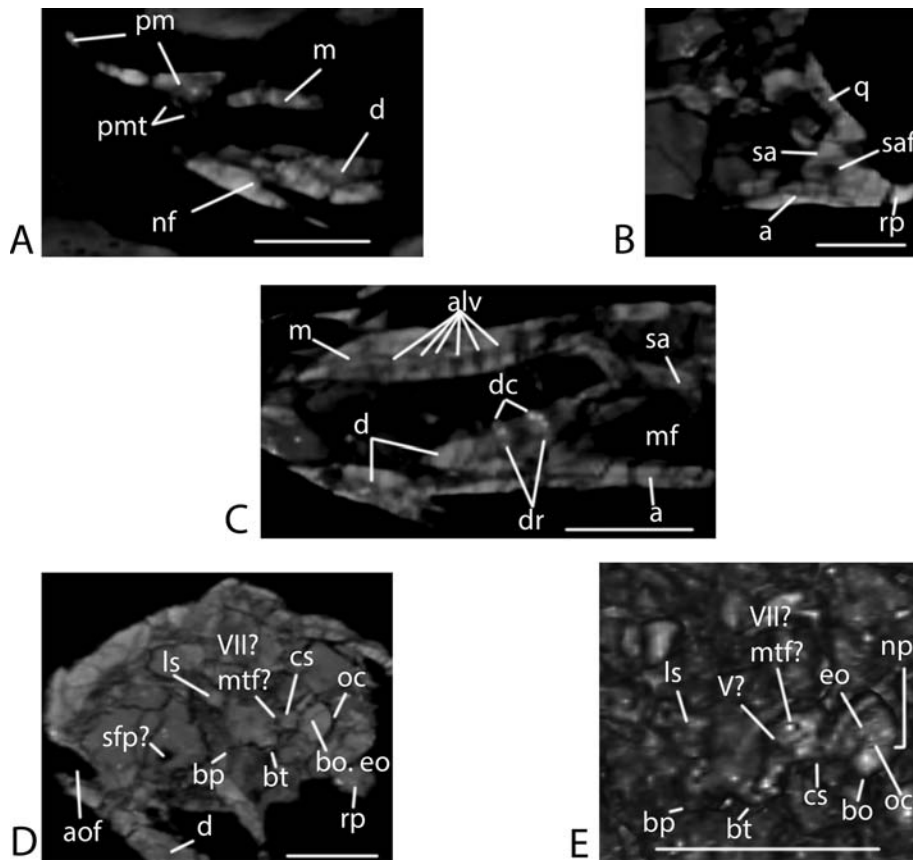


FIGURE 4. CT images of PEFO 38001. **A**, anteromedial surface of the right dentary and premaxilla; **B**, posterior portion of the medial surface of the right ramus of the mandible; **C**, medial surface of the right maxilla and dentary; **D**, braincase in posterolateral view; **E**, braincase in 3D reconstruction in a laterally oblique view. **Abbreviations:** a, angular; alv, alveoli; aof, antorbital fenestra; bo, basioccipital; bo, eo, basioccipital–exoccipital contact; bp, basiptyergoid process; bt, basal tuber; cs, condylar stalk; d, dentary; dc, dental crown; dr, dental root; eo, exoccipital; ls, laterosphenoid; m, maxilla; mf, mandibular fenestra; mtf, metotic foramen; nf, nutrient foramen; np, notochordal pit; oc, occipital condyle; pm, premaxilla; pmt, premaxillary teeth; q, quadrate; sa, surangular; saf, surangular foramen; sfp, suborbital fenestra of the palate; rp, retro-articular process; V, foramen for trigeminal nerve; VII, foramen for facial nerve. Scale bars equal 3 cm.

for a thorough descriptive comparison like the rest of the cranium; the laterosphenoid is only visible through the right orbit of the cranium (Fig. 3A). Alternatively, the braincase of PEFO 38001 was identified through CT imaging (Fig. 4D, E).

**Basioccipital**—Only part of the contact of the basioccipital with the exoccipital is discernible through CT imaging (Fig. 4D). Unlike the transversely ovate occipital condyle of *Scutarx deltatylus* (Parker, 2016b:fig. 8), the occipital condyle of PEFO 38001 is semicircular in posterior view (Fig. 4E) as seen in *Polesinesuchus aurelioi* (Roberto-Da-Silva et al., 2014:fig. 4), *Stagonolepis olenkae* (Sulej, 2010:fig. 5), and the isolated braincase of TTU-P 9214 described by Martz (2002:fig. 4.2); the condyle appears to be largely composed of the basioccipital (Fig. 4D), while the exoccipital composes part of the dorsal section, a condition seen in TTU-P 9214 and *Tecovasuchus chatterjeei* (Martz and Small, 2006:fig. 4a). Additionally, there is a shallow notochordal pit on the articular surface of the condyle (Fig. 4E); in *Stagonolepis olenkae* (Sulej, 2010) the notochordal pit is near the dorsal margin of the occipital condyle, while in *Polesinesuchus aurelioi* (Roberto-Da-Silva et al., 2014:fig. 4e) and PEFO 38001 the notochordal pit is toward the center of the articular surface of the occipital condyle.

In lateral view the stalk of the condyle is anteroposteriorly elongated (Fig. 4D), a condition seen in *Tecovasuchus chatterjeei* (Martz and Small, 2006:fig. 4), *Polesinesuchus aurelioi* (Roberto-Da-Silva et al., 2014), *Stagonolepis olenkae* (Sulej, 2010), and the braincase of TTU-P 9214 (Martz, 2002:fig. 4.2); this is the opposite of what we see in *Desmotosuchus smalli* (Small, 2002:fig. 6), which has an anteroposteriorly short condylar stalk, or in *Scutarx deltatylus* (Parker, 2016b:fig. 7), which has no distinctive ‘neck.’ Laterally, the ventral margin of the condylar stalk in PEFO

38001 is fairly straight (Fig. 4D) like that of *Stagonolepis olenkae* (Sulej, 2010), while in the isolated braincase of TTU-P 9214 (Martz, 2002:fig. 4.2) the ventral margin is gently curved; in *Stagonolepis robertsoni* (Walker, 1961:fig. 5), *Polesinesuchus aurelioi* (Roberto-Da-Silva et al., 2014:fig. 4), and *Tecovasuchus chatterjeei* (Martz and Small, 2006:fig. 4) the condylar stalk has a strongly concave ventral margin. From the anterior edge of the condylar neck the ventral margin of the basioccipital sharply descends as it meets the basal tuber (Fig. 4D, E); this is not seen in the isolated braincase of TTU-P 9214 (Martz, 2002:fig. 4.2) in which the margin gradually descends to the basal tubera.

**Parabasisphenoid**—The suture with the basioccipital is not discernible through CT imaging. The basiptyergoid processes are not elongate or laterally projected as in TTU-P 9214 (Martz, 2002:fig. 4.2). The most ventral margins of the basiptyergoid processes are nearly horizontal with that of the basal tubera (Fig. 4D); in both *Stagonolepis* species (*S. robertsoni* and *S. olenkae*; Walker, 1961:fig. 5; Sulej, 2010:fig. 5), *Scutarx deltatylus* (Parker, 2016b:fig. 9), *Tecovasuchus chatterjeei* (Martz and Small, 2006:fig. 4), and the isolated braincase (TTU-P 9214) described by Martz (2002) the basiptyergoid processes are significantly lower than the basal tubers. The ventral margin of the parabasisphenoid is strongly concave between the basal tuber and the basiptyergoid process in PEFO 38001 (Fig. 4E). This concavity is not seen in TTU-P 9214 (Martz, 2002), but it is seen in the braincases of both *Stagonolepis* species (*S. robertsoni* and *S. olenkae*; Walker, 1961:fig. 5; Sulej, 2010:fig. 5), *Scutarx deltatylus* (Parker, 2016b:fig. 9), *Tecovasuchus chatterjeei* (Martz and Small, 2006:fig. 4); the degree of this concavity varies within the mentioned taxa: the ventral margin is strongly concave

(e.g., *Stagonolepis robertsoni*; Walker, 1961), more moderate (e.g., *Stagonolepis olenkae* and *Scutarx deltatylus*; Sulej, 2010; Parker, 2016b), or gently concave (e.g., *Tecovasuchus chatterjeei*; Martz and Small, 2006).

**Prootic**—The prootic itself is not discernible in the CT imagery, but two visible foramina are assumed to be associated to the prootic based on their locations. Laterally, there is a foramen anterodorsally to the condylar stalk (Fig. 4D, E). This foramen is probably the exit of the facial nerve (CN VII), as described in the isolated braincase TTU-P 9214 by Martz (2002:fig. 4.2) but it could also represent the metotic foramen, as seen in *Polesinesuchus aurelioi* (Roberto-Da-Silva et al., 2014). Anteroventrally to that opening is another foramen (Fig. 4E), which most likely represents the exit of the trigeminal nerve (CN V); in TTU-P 9214 (Martz, 2002), *Stagonolepis olenkae* (Sulej, 2010), and *Desmatosuchus smalli* (Small, 2002) the foramen for CN VII and V are adjacent to each other.

### Mandible

Because the skull of PEFO 38001 has been laterally compressed and shifted, the right half (Fig. 3) shows the left half of the jaw being displaced ~4 cm horizontally and ~5 cm vertically. Both halves of the lower jaw are still joined at the mandibular symphysis (Fig. 3). Prior to deformation, the retroarticular processes would have been ~8 cm apart. Anteroposteriorly, the lower jaw is ~18 cm long, and is tallest dorsoventrally by the mandibular fenestra with a height of 3.5 cm. Because of the lateral compression, the prearticular has been pushed up onto the medial side of the internal mandibular fenestra. The anterior half of the fenestra is occupied by the prearticular. Laterally, the external mandibular fenestra is horizontally longer than dorsoventrally tall, with a length of 4.8 cm and a maximum height of ~1.8 cm; the length of the mandibular fenestra is nearly 33% of the total length of the jaw. The opening has a subtriangular shape, with its maximum height towards the middle.

**Dentary**—In lateral view, the dentary of PEFO 38001 (Fig. 3) makes up over 50% of the lower jaw with a length of 9.5 cm. This bone is mediolaterally compressed and slender, unlike that of *Desmatosuchus smalli* (Small, 2002) which is more robust. Like in *Stenomyti huangae* (Small and Martz, 2013), the posterior end of the dentary splits into two rami of equal length (Fig. 3B); unlike that of *Aetosauroides scagliai* (Biacchi Brust et al., 2018) and *Stagonolepis robertsoni* (Walker, 1961), which have a proportionately longer (anteroposteriorly) dorsal branch, or *Desmatosuchus smalli* (Small, 2002) which has a proportionately longer (anteroposteriorly) ventral branch. The contact between the posteroventral ramus of the dentary and the angular varies within Aetosauria (Desojo et al., 2013:fig. 4). *Paratyphothorax andressorum* (Schoch and Desojo, 2016), *Desmatosuchus smalli* (Small, 2002), *Stenomyti huangae* (Small and Martz, 2013), *Stagonolepis olenkae* (Sulej, 2010), *Neoaetosauroides engaeus* (Desojo and Báez, 2007), and *Aetosaurus ferratus* (Schoch, 2007) exhibit a prong-like contact with the angular as the branch tapers posteriorly. On the other hand, *Longosuchus meadei* (Parrish, 1994) and *Aetosauroides scagliai* (Biacchi Brust et al., 2018) have a relatively straight dorsoventral contact with the angular. The posteroventral ramus of *Typhothorax coccinarum* (PEFO 38001) composes the anterior 1.5 cm of the ventral margin of the external mandibular fenestra and overlaps the anteroventral process of the angular as it extends posterodorsally, giving it a broad curved contact (Fig. 3); the inverse condition is seen in *Stagonolepis robertsoni* (Walker, 1961), where the ventral ramus of the dentary is overlapped by the anterodorsal process of the angular.

The posterodorsal ramus of the dentary composes the anterior 1.8 cm of the anterodorsal margin of the external mandibular fenestra (Fig. 3B). Additionally, this branch has a simple (i.e.,

no overlap), slightly-curved dorsoventral contact with the surangular, a condition seen in *Desmatosuchus smalli* (Small, 2002); unlike the prong overlap seen in *Neoaetosauroides engaeus* (which is sharply S-shaped; Desojo and Báez, 2007), *Stenomyti huangae* (Small and Martz, 2013), *Aetosaurus ferratus* (Schoch, 2007), and both *Stagonolepis* species (*S. robertsoni* and *S. olenkae*; Walker, 1961; Sulej, 2010). The anteroventral margin of the dentary is not concave downwards (Fig. 3), as seen in stagonolepidoid aetosaurs, which have an angled 'chin' shape (Walker, 1961; Martz, 2002; Parker, 2018). The dentary gradually curves upwards in PEFO 38001, which matches the dentary of NMMNH P-12964 (Heckert et al., 2010:fig. 8a–c). This 'slipper'-shape dentary is also seen in the stagonolepidoid *Aetosauroides scagliai* (Biacchi Brust et al., 2018) and the early diverging typhothoracine *Aetosaurus ferratus* (Schoch, 2007). Ventrally, the dentary narrows upwards anteriorly by ~20° around the anterior fifth tooth and forms a beak; the first 3.0 cm of the dentary is edentulous. Posteriorly, the dentary is at its dorsoventrally broadest. There is no sign of contact on the lateral surface between the dentary and the splenial, similar to *Neoaetosauroides engaeus* (Desojo and Báez, 2007). Only the medial surface of the left ramus of the mandible (Fig. 3B) shows the straight medioventral contact between the dentary and the splenial.

The lateral surface of the dentary is covered in small foramina that are concentrated on the anterior half (Fig. 3). These foramina would have been occupied by fibers of the mandibular branch of the trigeminal nerve (CN V<sub>3</sub>; Desojo et al., 2013). The mandibular branch provides motor innervation to the jaw muscles of the mandibular arch as well as sensations from the mandible (Desojo and Báez, 2007; George and Holliday, 2013). This specimen of *Typhothorax coccinarum* (PEFO 38001) has a greater density of foramina in the dentary compared with that of *Neoaetosauroides engaeus* (Desojo and Báez, 2007), *Stagonolepis olenkae* (Sulej, 2010), or *Desmatosuchus smalli* (Small, 2002). CT imagery shows the Meckelian foramen on the medial surface (Fig. 4A), as described in TTU-P 9214 (Martz, 2002:fig. 4.3). The foramen is just behind the mandibular symphysis (Fig. 4A) in PEFO 38001; *Desmatosuchus smalli* (Small, 2002), *Neoaetosauroides engaeus* (Desojo and Báez, 2007), and TTU-P 9214 (Martz, 2002) have the Meckelian foramen at a similar position. Unlike an isolated dentary of TTU-P 9214 (Martz, 2002:fig. 4.3), which has 10 alveoli, the dentary of PEFO 38001 contains nine teeth; like the maxilla, the dentary also exhibits deep alveoli (Fig. 4C). There are no signs of interdental plates, tooth replacement, or wear facets on individual teeth.

**Angular**—Laterally, the angular of *Typhothorax coccinarum* (PEFO 38001) is a slender bone and is dorsoventrally thickest at its contact with the posterior margin of the external mandibular fenestra (Fig. 3). It extends (8.5 cm) from its contact with the dentary to the posterior border of the mandible, composing the posteroventral margin of the retroarticular process and the posterior-half of the ventral margin of the mandible (Fig. 3B); this extension is also seen in *Aetosaurus ferratus* (Schoch, 2007:fig. 9b) and *Longosuchus meadei* (Parrish, 1994), although the angular of *A. ferratus* descends posteriorly. In *Stenomyti huangae* (Small and Martz, 2013), *Desmatosuchus smalli* (tentatively; Small, 2002), *Paratyphothorax andressorum* (Schoch and Desojo, 2016), *Coahomasuchus chathamensis* (Heckert et al., 2017), *Neoaetosauroides engaeus* (Desojo and Báez, 2007), and both *Stagonolepis* species (*S. robertsoni* and *S. olenkae*; Walker, 1961; Sulej, 2010) the angular is not involved in the retroarticular process because it is posteriorly truncated by the surangular.

Laterally, the angular tapers anteroventrally as it receives the posteroventral ramus of the dentary. As commonly seen in other aetosaurs (Desojo et al., 2013:fig. 4; Schoch and Desojo 2016:fig. 7), including *Typhothorax coccinarum*, the dorsal

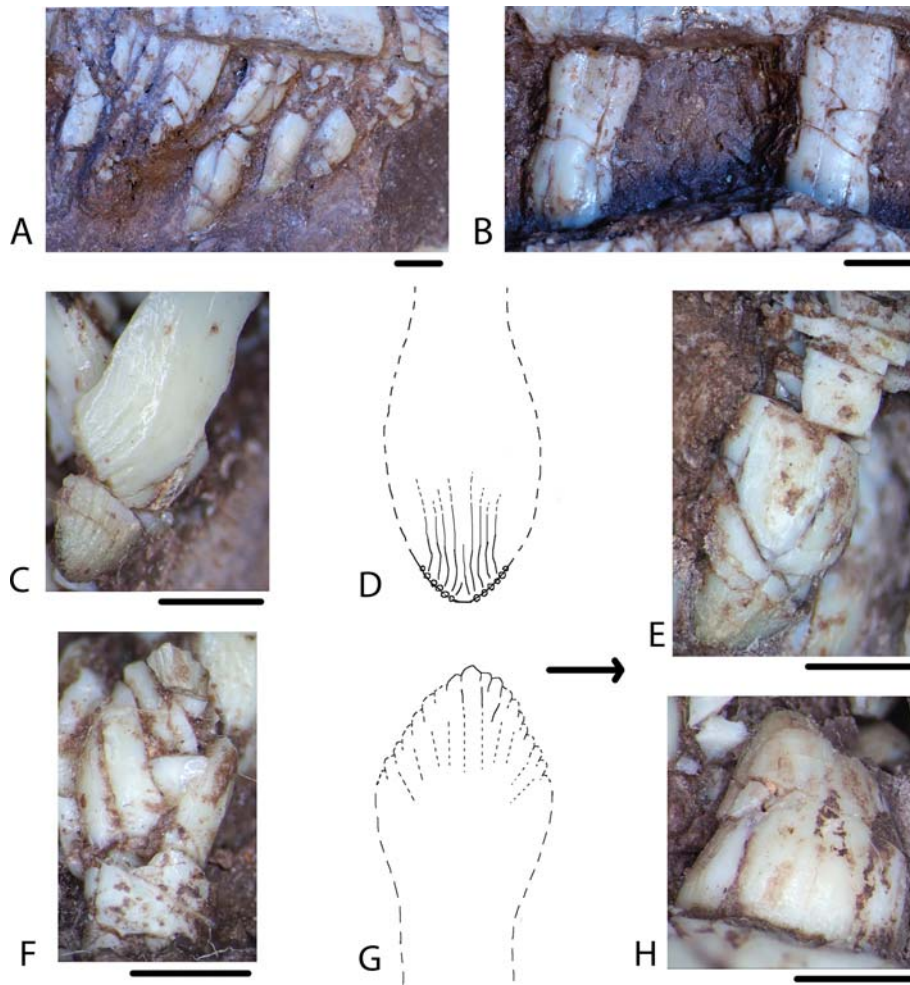


FIGURE 5. Dentition of PEFO 38001 in labial view. **A**, right premaxillary teeth; **B–E**, right maxillary teeth: **B**, anterior two teeth; **C**, **D**, posterior tooth with denticles and interpretive sketch, respectively; **E**, most posterior tooth; **F–H**, right dentary teeth: **F**, **G**, anterior rhomboidal-shaped tooth and interpretive sketch, respectively; **H**, posterior recurved tooth. Arrow indicates mesial direction. Scale bars equal 2 mm.

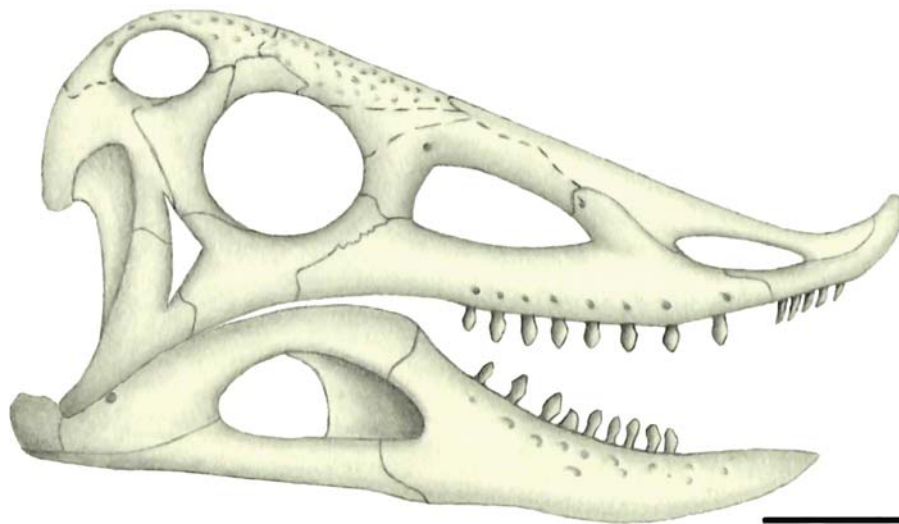


FIGURE 6. Skull illustration of *Typothorax coccinarum* based on PEFO 38001 in right lateral view. Scale bar equals 5 cm.

surface of the angular forms most of the ventral margin of the external mandibular fenestra (Fig. 3); *Coahomasuchus chathamensis* (Heckert et al., 2017:fig. 7) appears to be an exception, in which the angular is omitted from the margin of the external mandibular fenestra. Additionally, it has a broadly (anteroposteriorly) curved descending contact with the posteroventral margin of the surangular in lateral view, similar to that of *Longosuchus meadei* (Parrish, 1994). The angular becomes a long, thin process as it tapers posteriorly, underlying the ventral margin of articular in the retroarticular process. Medially, the angular contacts the posterior margin of the dentary and has a relatively straight (anteroposteriorly) dorsal contact with the ventral margin of the prearticular (Fig. 3B).

**Surangular**—In PEFO 38001, the surangular forms the majority of the lateral posterodorsal portion of the lower jaw and arches over the external mandibular fenestra (Fig. 3). Posteroventrally, it has a long (~5 cm) contact with the posterodorsal margin of the angular, nearly half the length of the surangular (Fig. 3B). Additionally, the ventral margin forms both the posterior and dorsal margins of the external mandibular fenestra; the surangular does not descend as a short anterior process along the dorsal edge of the angular at the posterior end of the external mandibular fenestra, a condition seen in *Stenomyti huangae* (Small and Martz, 2013), *Paratyphothorax andressorum* (Schoch and Desojo, 2016), *Aetosaurus ferratus* (Schoch, 2007), *Longosuchus meadei* (Parrish, 1994), *Neoaetosauroides engaeus* (Desojo and Báez, 2007), and both *Stagonolepis* species (*S. robertsoni* and *S. olenkae*; Walker, 1961; Sulej, 2010).

The posterior margin of the surangular has a slightly curved dorsoventral contact with the articular (Fig. 3B). The surangular is minimally involved towards the anterior of the retroarticular process and does not participate in the ventral margin of the mandible (Fig. 3); this is unlike the condition seen in *Neoaetosauroides engaeus* (Desojo and Báez, 2007), *Coahomasuchus chathamensis* (Heckert et al., 2017), *Longosuchus meadei* (Parrish, 1994), *Aetosaurus ferratus* (Schoch, 2007), *Paratyphothorax andressorum* (Schoch and Desojo, 2016), *Desmatosuchus smalli* (Small, 2002), *Stenomyti huangae* (Small and Martz, 2013), and both *Stagonolepis* species (*S. robertsoni* and *S. olenkae*; Walker, 1961; Sulej, 2010) in which the posterior projection of the surangular composes most of the body of the retroarticular process, while forming the most posteroventral margin of the mandible.

The surangular foramen is visible on both the lateral (Fig. 3B) and medial surfaces (Fig. 4B) of the posterior end of the surangular. They are connected internally by a channel that was filled by fibers of the inferior alveolar nerve (Desojo et al., 2013), which is also described in *Neoaetosauroides engaeus* (Desojo and Báez, 2007), *Paratyphothorax andressorum* (Schoch and Desojo, 2016), and *Desmatosuchus smalli* (Small, 2002). The inferior alveolar nerve is a derivative of the mandibular branch of the trigeminal nerve that supplies sensation to the teeth in the dentary (Desojo and Báez, 2007). There is no sign of an ascending flange towards the posterodorsal margin of the surangular, as described in *Stagonolepis robertsoni* (Walker, 1961).

**Articular**—The articular of *Typhothorax coccinarum* is large in lateral view and is greatly involved in the body of the retroarticular process (Fig. 3B), similar to that of *Paratyphothorax andressorum* (Schoch and Desojo, 2016), *Stagonolepis robertsoni* (Walker, 1961), and *Aetosaurus ferratus* (Schoch, 2007). The dimensions and shape of the articular varies among aetosaurs (Desojo et al., 2013): some are as dorsoventrally tall as anteroposteriorly wide in lateral view (e.g., *Stagonolepis olenkae*; Sulej, 2010:fig. 7b), wider than tall and square-shaped in lateral view as seen in PEFO 38001, taller than wide and triangular in lateral view (e.g., *Paratyphothorax andressorum*; Schoch and Desojo, 2016:fig. 7a), or so greatly reduced that it is absent in lateral view (e.g., *Neoaetosauroides engaeus*; Desojo and Báez,

2007). The articular is bounded by both the surangular (anteriorly) and angular (ventrally) in PEFO 38001 (Fig. 3B); this has not been described in any other aetosaur species, suggesting that this might be an apomorphic character of *Typhothorax coccinarum*. The articular is also visible medially on the left ramus of the mandible (Fig. 3B), but the left articular is not as dorsally curved as the articular on the right ramus. No medial contacts of the articular are discernible in PEFO 38001.

**Splénial**—The splénial is visible on the medial surface of the left jaw (Fig. 3B). The splénial is a long flat bone with an anteroposterior length of ~6.5 cm that ventrally overlaps the medial surface of the dentary and the anterior region of the medial surface of the prearticular towards its posterior, as seen in *Desmatosuchus smalli* (Small, 2002). The ventral margin of the splénial in PEFO 38001 is not visible in lateral view. This differs from *Neoaetosauroides engaeus* (Desojo and Báez, 2007), *Desmatosuchus smalli* (Small, 2002), *Stenomyti huangae* (Small and Martz, 2013), *Aetosaurus ferratus* (Schoch, 2007), *Paratyphothorax andressorum* (Schoch and Desojo, 2016), *Longosuchus meadei* (Parrish, 1994), *Aetosauroides scagliai* (Biacchi Brust et al., 2018), and both *Stagonolepis* species (*S. robertsoni* and *S. olenkae*; Walker, 1961; Sulej, 2010), which all have the splénial laterally exposed on the ventral margin of the mandible contacting the dentary.

**Prearticular**—Part of the prearticular is visible on the medial surface of the left ramus of the mandible and forms much of the medial wall on the posterior portion of the jaw (Fig. 3B). The posterodorsal section of the prearticular is laterally visible through the external mandibular fenestra. Anteriorly, the prearticular is overlapped by the splénial. Ventrally, it contacts the medial border of the angular. Posteriorly, the suture between the prearticular and articular is not discernible.

## Dentition

**Premaxillary Teeth**—The posterior half of the right premaxilla of PEFO 38001 appears to bear five teeth, but only the three anterior premaxillary teeth are describable (Fig. 5A); no teeth are preserved in the left premaxilla (Fig. 2). Premaxillary tooth count varies within Aetosauria (Desojo et al., 2013:fig. 4): the premaxilla of *Desmatosuchus smalli* (Small, 2002) is edentulous, that of *Aetosauroides scagliai* (Biacchi Brust et al., 2018) and *Stagonolepis robertsoni* (based on alveoli count; Walker, 1961) contain five teeth, that of *Aetosaurus ferratus* (Schoch, 2007) and *Neoaetosauroides engaeus* (Desojo and Báez, 2007) contain four teeth, and that of *Stenomyti huangae* (Small and Martz, 2013) contains three teeth. The premaxillary teeth of PEFO 38001 increase in their overall size posteriorly (Fig. 5A); the largest tooth has an apicobasal height of ~6 mm and a mesiodistal width of ~3 mm. The premaxillary teeth are each separated by ~1 mm and are labiolingually compressed, unlike the conical teeth of *Neoaetosauroides engaeus* (Desojo and Báez, 2007:fig. 3) and *Stenomyti huangae* (Small and Martz, 2013:fig. 4a); similarly, the premaxillary teeth in *Stagonolepis robertsoni* (Walker, 1961) are also labiolingually compressed, but only towards the crown apex.

The base of the anterior two premaxillary teeth are crushed but that of the posterior three are intact (Fig. 5A). The second and third teeth are slightly recurved distally near the apices and have curved tips, similar to *Aetosaurus ferratus* (Schoch, 2007:fig. 8a). In comparison, *Aetosauroides scagliai* (Biacchi Brust et al., 2018:fig. 2c) and *Paratyphothorax andressorum* (Schoch and Desojo, 2016:fig. 4b) also have distally recurved premaxillary teeth, but their apices are not curved; the curvature in *Aetosauroides scagliai* (Biacchi Brust et al., 2018) is slight near the apex and most of the distal margin remains straight apicobasally, while in *Paratyphothorax andressorum* (Schoch and Desojo, 2016) the distal margin is slightly curved apicobasally. Additionally, the mesial margin of the premaxillary teeth in PEFO 38001

straightens just below the apex until it slenders at the neck; in *Aetosauroides scagliai* (Biacchi Brust et al., 2018:fig. 4b) the mesial margin is mainly straight apicobasally, while in *Paratytophorax andressorum* (Schoch and Desojo, 2016:fig. 7a) the mesial margin is slightly curved. Vertical fluting is visible on the labial surface near the apex of the second and third pre-maxillary teeth; there is no evidence of serrations or wear facets.

**Maxillary Teeth**—The maxillae of PEFO 38001 contain eight alveoli, but only four maxillary teeth are preserved in each. The first four anterior teeth are well preserved on the left maxilla (Fig. 2). The right maxilla (Fig. 3) preserves the two most anterior (Fig. 5B) and two posterior teeth (Fig. 5C–E). The remaining four teeth near the center of the right maxilla are crushed (Fig. 3). Based on the preserved maxillary teeth (Fig. 5B–E) and CT imaging (Fig. 4C), the teeth have a thecodont implantation and are deeply rooted in their alveoli; most began to fall out of their alveoli during burial, exposing most of the root. The two most anterior teeth (Fig. 5B) have a total height of 1.2 cm and are apicobasally taller compared with the maxillary teeth on the left maxilla (Fig. 2), which are *in situ* and have an apicobasal height of ~4–6 mm. The difference in height is due to the right maxillary teeth slightly falling out of their alveoli; from the constricted base to the apex, the apicobasal height of the the right maxillary teeth is ~4 mm. The two posterior teeth on the right maxilla (Fig. 5C–E) have a height of ~7 mm. All the maxillary teeth have a mesiodistal width of ~3–4 mm, which is proportionately low compared with the maxillary teeth of *Desmatosuchus smalli* (Small, 2002:fig. 9), *Stagonolepis olenkae* (Sulej, 2010:fig. 2i), and *Paratytophorax andressorum* (Schoch and Desojo, 2016:fig. 5). The intradental gap decreases posteriorly from ~8 mm to ~2–3 mm.

In labial view, the maxillary teeth have an almond-shaped outline with a constriction between the root and crown (Figs. 2A, 5C–E); both the mesial and distal margins gently curve to a rounded tip, as seen in *Aetosaurus ferratus* (Schoch, 2007:fig. 9a), *Stenomyti huangae* (Small and Martz, 2013:fig. 4b), and *Stagonolepis olenkae* (albeit the tips meet at a point; Sulej, 2010:fig. 8b). In comparison, the maxillary tooth outline of *Desmatosuchus smalli* (Small, 2002:fig. 2a) and *Stagonolepis robertsoni* (Walker, 1961:fig. 2b) is rhomboidal-shaped with a constricted crown base (Schoch and Desojo, 2016:fig. 8e–g). The maxillary teeth of *Tytophorax coccinarum* are not strongly recurved like those of *Aetosauroides scagliai* (Desojo and Ezcurra, 2011; Biacchi Brust et al., 2018:fig. 6). The lingual surfaces of the teeth are not visible in PEFO 38001. The lingual surface could possibly be flat while the labial surface is slightly bulbous; in cross-section this would appear as an almost straight lingual margin and a curved labial margin.

The anterior maxillary teeth have long roots and are labiolingually compressed towards the base on the right maxilla (Fig. 5B); they are not conical and thus unlike those of *Longosuchus meadei* (Parrish, 1994:fig. 1) or *Neoaetosauroides engaeus* (Desojo and Báez, 2007:fig. 3c). The second-to-last posterior tooth (Fig. 5C, D) has rounded denticles on the carina towards the apex, similar to the maxillary teeth of *Revueltosaurus callenderi* (Heckert, 2002:fig. 4), but not as prominent. The most posterior tooth on the right maxilla (Fig. 5E) has a slightly different morphology from the anterior maxillary teeth; it is more bulbous and appears to have a mesiodistally narrower, constricted neck. The maxillary teeth are not serrated like those of *Aetosauroides scagliai* (Desojo and Ezcurra, 2011; Biacchi Brust et al., 2018:fig. 6). None of the anterior maxillary teeth from either side have denticles on their margins. All of the preserved maxillary teeth have vertical fluting towards the apices (Fig. 5B–E); the maxillary teeth appear uniform in shape, but exhibit variation in texture with the presence/absence of denticles. There are no signs of wear facets or tooth replacement.

**Dentary Teeth**—While most of the teeth are crushed on the right dentary, the dentary of this specimen of *Tytophorax coccinarum* has nine identifiable teeth (Fig. 3), whereas an isolated dentary of TTU-P 9214 (Martz, 2002:fig. 4.3) has alveoli for ten. The teeth are tightly spaced, which compares favorably with the intradental spacing of the alveoli seen in TTU-P 9214 (Martz, 2002:fig. 4.3). Additionally, the CT scan also shows that like the maxillary teeth, the dentary teeth have large roots and are deeply rooted within their alveoli (Fig. 4C). The dentary of PEFO 38001 is weakly heterodont and exhibits two distinct tooth morphologies (Fig. 5F–H). Based on one preserved anterior tooth (Fig. 5F, G) that is *in situ*, most of the dentary teeth are similar to those of *Desmatosuchus smalli* (Small, 2002:fig. 2) and *Stagonolepis robertsoni* (Walker, 1961:fig. 6), but are not as robust and have more gently curved margins; the crown apex is labiolingually compressed, mesiodistally constricted at the base, and become more rhomboidal-shaped apically with evidence of fluting at the apex (Fig. 5F, G). For comparison, *Neoaetosauroides engeus* (Desojo and Báez, 2007:fig. 4), *Aetosaurus ferratus* (Schoch, 2007:fig. 9b), and *Stenomyti huangae* (Small and Martz, 2013:fig. 7b) also have dentary teeth with mesiodistally compressed bases, but their teeth are bulbous as opposed to labiolingually compressed, as seen in PEFO 38001. These rhomboidal-shaped teeth (Fig. 5F–G) have an apicobasal height of ~5–6 mm, and mesiodistal widths of ~2 mm at the base and ~3 mm just before it slenders to a curved tip.

On the other hand, an *in situ* tooth near the posterior end of the dentary (Fig. 5H) is apicobasally shorter than the rhomboidal-shaped anterior tooth with a height of ~4 mm and has an unconstricted base with a mesiodistal width of ~3 mm. The tooth is labiolingually compressed, but the labial surface exhibits a bulbous curvature. The mesial margin of this tooth is strongly convex, while the distal margin is gently curved (Fig. 5H). Additionally, the tooth has a curved apex; this apex is positioned mesial to the vertical plane from the most distal edge of the base. The dentary teeth of *Aetosauroides scagliai* (Desojo and Ezcurra, 2011; Biacchi Brust et al., 2018:fig. 2) exhibit a similar distally curved tooth morphology, but are very labiolingually compressed, apicobasally taller with straighter margins, and have a uniform mesiodistal width from the base to just below the crown apex; *Stenomyti huangae* (DMNH 61392; Small and Martz, 2013:fig. 7b) also has a similar tooth towards the posterior of its dentary, but it has a constricted base. Unlike the anterior dentary tooth (Fig. 5F, G), there is no sign of textured ridges (Fig. 5H). No teeth are visible for identification on the left dentary, because the left half of the mandible is shut (Fig. 2). There is no evidence of wear facets, or details of tooth replacement.

## DISCUSSION

The skull of PEFO 38001 (Fig. 6) is very important because it provides clarity on the cranial evolution of the Aetosauria (Fig. 7), specifically the Tytophoracinae and *Tytophorax coccinarum*. Most of our understanding of *Tytophorax coccinarum* is based on described postcranial elements (i.e., osteoderms and pelvic elements) and very few skull materials (Long and Murry, 1995; Heckert et al., 2010; Parker, 2013); although Heckert et al. (2010:636) argues that TTU-P 9214 could possibly refer to a different taxon based on the variations between TTU-P 9214 and that of other specimens of *Tytophorax coccinarum*, we believe that TTU-P 9214 is indeed a juvenile specimen of *Tytophorax coccinarum* and that the variations are most likely ontogenetic as described by Martz (2002). Based on PEFO 38001 (Fig. 6), an isolated maxilla (PEFO 42506), NMMNH P-12964 (Heckert et al., 2010:figs. 6–9), and an isolated dentary and braincase (TTU-P 9214; Martz, 2002:figs. 4.2–4.3), the skull of *Tytophorax coccinarum* is gracile in nature with

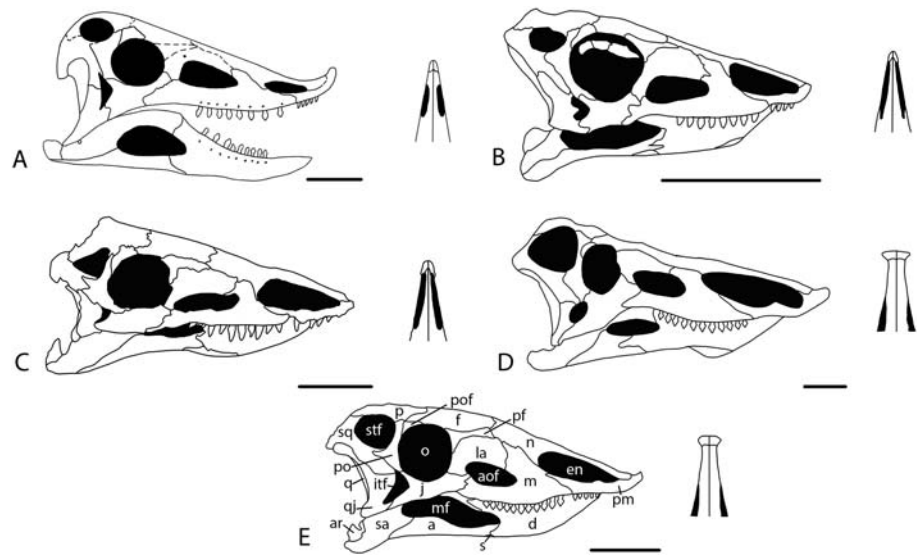


FIGURE 7. Skulls of selected aetosaurs in right lateral view and dorsal view of their respective snouts (modified from Schoch and Desojo, 2016). **A**, *Tytophorax coccinarum*; **B**, *Aetosaurus ferratus*; **C**, *Paratytophorax andressorum*; **D**, *Desmatosuchus smalli*; **E**, *Stagonolepis robertsoni*. **Abbreviations**: a, angular; aof, antorbital fenestra; ar, articular; d, dentary; en, external naris; f, frontal; itf, infratemporal fenestra; j, jugal; la, lacrimal; m, maxilla; mf, mandibular fenestra; n, nasal; o, orbit; p, parietal; pf, prefrontal; pm, premaxilla; po, postorbital; pof, postfrontal; q, quadrate; qj, quadratojugal; s, splenial; sa, surangular; sq, squamosal; stf, supratemporal fenestra. Scale bars equal 5 cm.

mediolaterally thin bones. For comparison, the holotype skull of *Scutarx deltatylus* (PEFO 34616; Parker, 2016b) is similar in size to that of PEFO 38001, but has a dorsoventrally thickened skull roof making it more robust than that of *Tytophorax coccinarum*. The gracile nature of the skull of *Tytophorax coccinarum* (Fig. 3) might explain the lack of skull material in the fossil record for tytophoracines.

In reconstruction, the skull of *Tytophorax coccinarum* is notably small for its body size (Long and Murry, 1995:fig. 99; Heckert et al., 2010:fig. 9), especially when compared with figures of other aetosaurian taxa (Fig. 7; Desojo et al., 2013:fig. 3). For comparison, the following proportions are based on measurements from published reconstructions of *Desmatosuchus smalli* (Small, 2002:fig. 2; Martz et al., 2013:figs. 10m–n), *Desmatosuchus spurensis* (Parker, 2008:fig. 34), *Longosuchus meadei* (Sawin, 1947:figs. 12, 13; Parrish, 1994:fig. 2), *Stagonolepis robertsoni* (Walker, 1961:figs. 22, 23), and the articulated skeleton of *Tytophorax coccinarum* (NMMNH P-12964) described by Heckert et al. (2010:fig. 9). We provide measurements in the Supplemental Data 1: (1) The anteroposterior length of the cranium relative to that of the entire body: ~12% in *D. smalli*, ~11% in *D. spurensis*, ~10% in *T. coccinarum* and *S. robertsoni*, and ~8% in *L. meadei*; (2) the transverse width in dorsal view of the widest section of cranium relative to that of the widest section of the trunk (or from base-to-base of the lateral projections, if any): ~38% in *S. robertsoni*, ~33% in *D. smalli*, ~32% in *D. spurensis*, ~30% in *L. meadei*, and ~17% in *T. coccinarum*. It should be noted that *Stagonolepis olenkae* (Sulej, 2010) is assumed to have a very similar postcranial skeleton (including skull-to-body size proportions) to that of *S. robertsoni* (Walker, 1961; Parker, 2016a; Drózd, 2018).

Based on these measurements it becomes apparent that *Tytophorax coccinarum* has a significantly smaller skull to body-size ratio (particularly in the transverse width in dorsal view) when compared to that of stagonolepidoid aetosaurs (Desojo et al., 2013:figs. 3e–k; Parker, 2016a). Additionally, based on the skull-to-body proportions of NMMNH P-12964 (Heckert et al., 2010), the skeleton belonging to this skull of PEFO 38001 should have a body length of ~2.1 m and a maximum dorsolateral width of ~53 cm at the trunk; this suggests that this specimen of *Tytophorax coccinarum* (Fig. 6; PEFO 38001) is slightly smaller and less skeletally mature than the NMMNH P-12964 specimen described by Heckert et al. (2010).

Although the features of the braincase of PEFO 38001 are only identifiable through CT imaging (Fig. 4D, E), there are some distinct differences between it and the isolated braincase of TTU-P 9214 (Martz, 2002:fig. 4.2). The major differences include: the length of the condylar stalk, the lateral ventral margin of the condylar stalk, and the lateral ventral margin of the parabasisphenoid between the basal tuber and basiptyergoid process (Fig. 4D, E). The mediolateral compression of the skull has distorted the braincase, which could explain the variation between the braincase of PEFO 38001 (Fig. 4E) and that of TTU-P 9214 (Martz, 2002). Another hypothesis is that the two specimens are at a different ontogenetic stage of their growth; Martz (2002) described TTU-P 9214 as a juvenile specimen of *Tytophorax coccinarum*. Based on the reconstruction of Martz (2002:fig. 4.41) TTU-P 9214 would have an anteroposterior length of ~1.75 m; this makes it smaller and potentially less skeletally mature than PEFO 38001, which would have a total anteroposterior length of ~2.1 m (based on the skull-to-body proportions mentioned above). Further preparation of the postcrania (particularly that of the limbs) of PEFO 38001 is required to make a more thorough comparison to TTU-P 9214 (Martz, 2002) and the other articulated skeletons of *Tytophorax coccinarum* (NMMNH P-12964; NMMNH P-56299; Heckert et al., 2010:figs. 2–9).

Prior to the discovery of PEFO 38001, Small (2002) hypothesized that the skull morphology of *Tytophorax coccinarum* would have been similar to that of *Desmatosuchus smalli* (Small, 2002), in which the premaxillae are transversely expanded and edentulous, and most reconstructions of *Tytophorax coccinarum* present these characters (Long and Murry, 1995:fig. 99; Martz, 2002:fig. 4.41). Indeed, even the discovery of cranial material in the articulated skeleton of *Tytophorax coccinarum* (NMMNH P-12964; Heckert et al., 2010:fig. 9) did not change this hypothesis. The skull of PEFO 38001 (Fig. 6) demonstrates that these historic reconstructions of *Tytophorax coccinarum* are inaccurate. Instead, the premaxillae of *Tytophorax coccinarum* (PEFO 38001) each bear five teeth (Fig. 5A) and narrow anteriorly into a tip (i.e., tapered-snout), a condition also seen in other aetosaurines (Parker 2016a) such as *Stenomyti huangae* (Small and Martz, 2013:figs. 3, 11c), *Aetosaurus ferratus* (Fig. 7B; Schoch, 2007), and *Paratytophorax andressorum* (Fig. 7C; Schoch and Desojo, 2016). Although the premaxillae of PEFO 38001 join anteriorly into a tip (Fig. 7A),

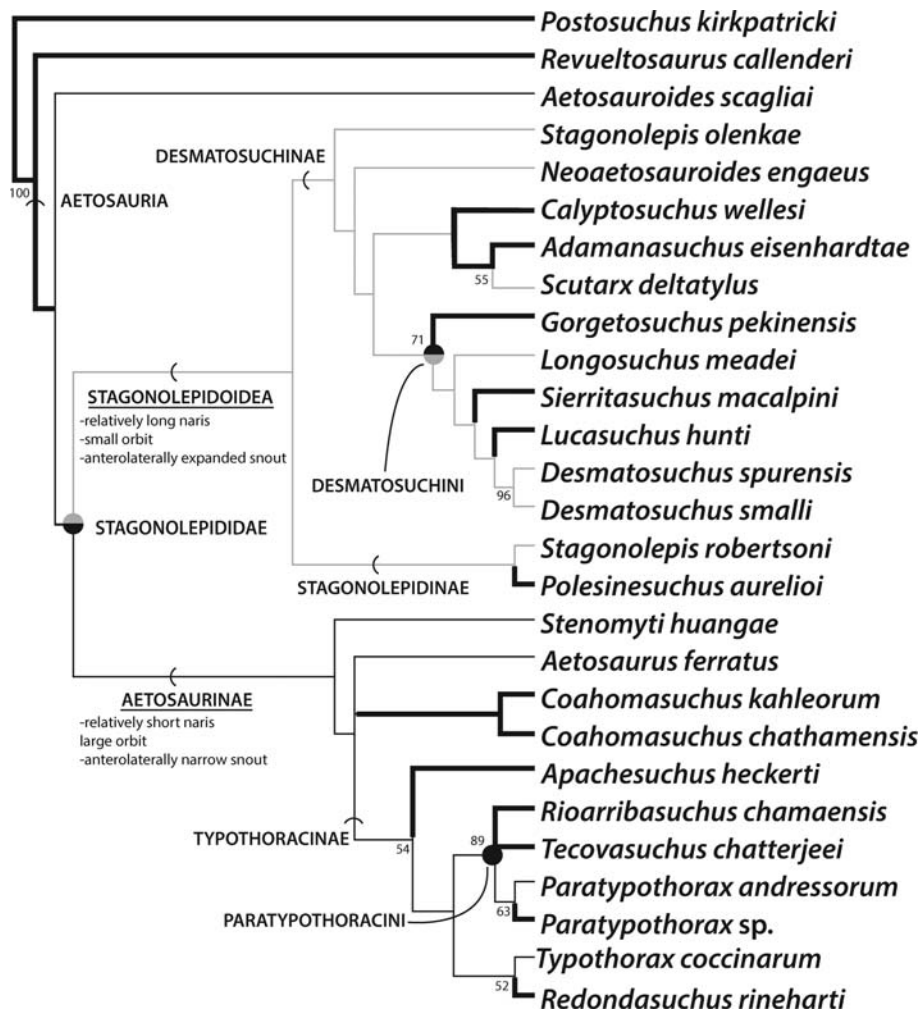


FIGURE 8: Skull morphotype optimizations mapped onto the strict consensus tree from the phylogenetic analysis (MPTs = 2, L = 233) showing the optimization of these character states within Aetosauria. Light gray shows the robust morphotype as described in the text. Thin black shows the gracile morphotype. Bold black indicates where cranial material is unknown or too incomplete. Absolute bootstrap frequencies <50% occur next to the respective node.

as in *Aetosaurus ferratus* (Fig. 7B; Schoch, 2007), the snout tip curves dorsally and forms an elongated process (Fig. 6). This feature is not seen in other aetosaurian taxa (Fig. 7), indicating that this dorsally recurved process of the premaxilla is possibly apomorphic to *Typosuchus coccinarum*. Also, the absence of a ‘chin’ (Fig. 3B) on the anteroventral margin of the dentary (sensu Walker, 1961) and the lack of a strongly downturned jugal (sensu Long and Murry, 1995) support its placement outside of Stagonolepidoidea (Parker, 2016a). These characters are also visible on the cast of the articulated *Typosuchus coccinarum* specimen (NMMNH P-12964) figured by Hunt et al. (1993:fig. 2a) and Heckert et al. (2010:fig. 8a–c), but the skull of this specimen has not been described in detail.

In addition to the differences (mentioned above) in morphology of the premaxilla, dentary, and jugal between PEFO 38001 and stagonolepidoidean aetosaurs, *Typosuchus coccinarum* exhibits relatively small external nares (Fig. 6). In *Desmatosuchus smalli* (Small, 2002), *Longosuchus meadei* (Parrish, 1994), *Neoaetosauroides engaeus* (Desojo and Báez, 2007), and in both species of *Stagonolepis* (*S. olenkae* and *S. robertsoni*; Walker, 1961; Sulej, 2010) the external naris is proportionately (relative to the orbit) the longest cranial opening (by a difference of ~3 cm) with an anteroposterior length that is ~25% that of the cranium (Fig. 7D, E); measurements are

provided in the Supplemental Data 1. The external naris in the skull of *Typosuchus coccinarum* (PEFO 38001) is roughly the same length as the orbit (~3.5 cm) and is ~17% the length of the cranium (Figs. 2, 6). *Stenomyti huangae* (Small and Martz, 2013:fig. 11), *Aetosaurus ferratus* (Schoch, 2007:fig. 8), and *Paratypothorax andressorum* (Schoch and Desojo, 2016:fig. 4), also have an external naris that is roughly the same length (or just slightly larger by ~1 cm) as the orbit (Fig. 7B, C), demonstrating this is an aetosaurine (sensu Parker, 2016a) synapomorphy; measurements are provided in the Supplemental Data 1.

### Phylogenetic analysis

To test the distribution of some of these new characters, and also to reflect recent changes in aetosaur taxonomy, we modified the phylogenetic analysis of Parker (2016a) by adding *Coahomasuchus chathamensis* (Heckert et al., 2017; Hoffman et al., 2018), combining SMNS 19003 with *Paratypothorax andressorum* (Schoch and Desojo, 2016), and adding ten new characters (nine cranial) including five characters from Schoch and Desojo (2016). The new matrix of 28 taxa and 93 characters (44 cranial, 49 non-cranial; Supplemental Data 2) was analyzed in TNT v1.5 (Goloboff et al., 2008) with 1,000 replications, random sequence addition, and tree bisection reconnection



swapping while keeping ten trees per replication and condensing zero-length branches (see Parker, 2016a); 13 characters (3, 4, 14, 20, 22, 23, 28, 64, 70, 73, 76, 79, 83) were ordered. Analytical instructions are provided in Supplemental Data 2. We a priori omitted the taxon *Aetobarbakinoides brasiliensis* because it acts as a wildcard taxon as determined by the previous Adams consensus tree of the parent data set (Parker 2016a). Our analysis resulted in two most-parsimonious trees (MPTs) with a length of 233 steps, a Consistency Index of 0.562 and a Retention Index of 0.715. The strict consensus of these two MPTs is shown in Fig. 8, with absolute bootstrap frequencies >50% (1,000 subsampled replicates). The results are nearly identical to that recovered by Parker (2016a:fig. 7), including the same clades. The addition of ten additional non-osteoderm characters did not alter the phylogenetic relationships of aetosaurus (see discussion in Parker, 2016a and Hoffman et al., 2018). We mapped the major skull types on this cladogram to show their distributions (Fig. 8).

Stagonolepidoid aetosaurus (Fig. 8) with preserved cranial material share a relatively long external naris, small orbit, and an anterolaterally expanded snout (Fig. 7D, E). On the other hand, aetosaurines (Fig. 8) share an external naris that is relatively small (equal to or with a difference of ~1 cm in length relative to the orbit), large orbit, and an anteriorly narrow tapered-shaped snout (Fig. 7A–C). Based on our phylogenetic reassessment of the Aetosauria (Fig. 8), two trends become apparent: (1) stagonolepidoids with a large external naris and very well-developed shovel-shaped snouts are restricted to the late Carnian and mid-Norian (i.e., Adamanian land vertebrate holochronozone; sensu Parker and Martz, 2011). Additionally, (2) the late Norian and early Rhaetian (i.e., Revueltian land vertebrate holochronozone; sensu Parker and Martz, 2011) is dominated by aetosaurine aetosaurus that share a small external naris and tapered-shaped snout. Sulej (2010) noted that the shape of the snout changed during aetosaur evolution. It is possible that the cranial proportion of the external nares and snout morphology are correlated characters within Aetosauria (Desojo et al., 2013:fig. 4).

### Feeding Ecology

Walker (1961) argued that aetosaurus were predominantly herbivorous and used their highly specialized skulls and stout forelimbs to dig into the soft soil and feed on the vegetation. Within the last decade, known skull material for aetosaurians has increased significantly including that of *Aetosauroides scagliai* (Biacchi Brust et al., 2018), *Scutarx deltatylus* (Parker, 2016a), *Paratytophorax andressorum* (Schoch and Desojo, 2016), *Stagonolepis olenkae* (Sulej, 2010), *Stenomylti huangae* (Small and Martz, 2013), *Coahomasuchus chathamensis* (Heckert et al., 2017), and now *Tytophorax coccinarum* (Fig. 6; PEFO 38001). The disparity in dentition types (Figs. 5, 7) within these skulls indicates that there is a potential variation in diet within Aetosauria, ranging from herbivory, insectivory, omnivory, and carnivory (Desojo and Vizcaíno, 2009; Desojo et al., 2013). *Aetosauroides scagliai* (Biacchi Brust et al., 2018), *Stagonolepis olenkae* (Sulej, 2010), *Paratytophorax andressorum* (Schoch and Desojo, 2016), and *Desmatosuchus smalli* (Small, 2002) are characterized by having homodont teeth, while the skull of PEFO 38001 (Fig. 3) indicates that *Tytophorax coccinarum* was becoming more heterodont by having at least one tooth (Fig. 5H) with a distinct morphology from the rest in its dentary (Fig. 5F–G), which has not been described in other aetosaur taxa.

The maxillary dentition of *Tytophorax coccinarum* (Fig. 5B–E) is not serrated like that of *Aetosauroides scagliai* (Biacchi Brust et al., 2018:fig. 6), but it shares morphological features with other aetosaur and non-aetosaur taxa. The maxillary dentition of PEFO 38001 (Figs. 2, 5C–E) is composed of labiolingually

compressed teeth, with mesiodistally constricted bases, and margins that converge into rounded apices; these characters are seen in the dentitions of *Aetosaurus ferratus* (Schoch, 2007: fig. 4), *Stenomylti huangae* (Small and Martz, 2013:fig. 4b), and *Stagonolepis olenkae* (Sulej, 2010:fig. 8b). The maxillary dentition of PEFO 38001 also includes a tooth with denticles (Fig. 5C, D) similar to those of *Revueltosaurus callenderi* (Heckert, 2002:figs. 2–4). These tooth morphologies have been hypothesized to indicate an herbivorous diet (e.g., Walker, 1961). Additionally, the dentary dentition is composed of teeth that are rhomboidal-shaped (Fig. 5F, G), similar to those of *Desmatosuchus smalli* (Small, 2002:figs. 2, 9) and *Stagonolepis robertsoni* (Walker, 1961:figs. 2, 6), and also includes a distally curved posterior tooth (Fig. 5H); *Stenomylti huangae* (DMNH 61392; Small and Martz, 2013:figs. 7, 11) exhibits a similar tooth morphology in its dentary but with a constricted base. The overall tooth morphologies support Small's (2002) hypothesis that compares modern armadillos to aetosaurus in which both clades are insectivorous or omnivorous, rather than strictly herbivorous (Desojo and Vizcaíno, 2009; Sulej, 2010; Desojo et al., 2013).

Heckert et al. (2010) applied Hildebrand's (1974) characteristics of digging tetrapods and Benton's (1983) thorough study of the Upper Triassic rhynchosaur *Hyperodapedon gordonii* to the articulated skeletons of *Tytophorax coccinarum* (NMMNH P-56299; NMMNH P-12969). Heckert et al. (2010) hypothesized that *Tytophorax coccinarum* might have engaged in forelimb scratch-digging in addition to snout-digging, using a shovel-shaped snout to unearth roots or burrowing animals (Desojo et al., 2013); based on the recent discovery of forelimb material, this hypothesis has also been suggested as an adaptation of *Stagonolepis olenkae* (Sulej, 2010; Drózd, 2018). It is not likely that *Tytophorax coccinarum* used its snout to engage in digging because the premaxillae are not transversely expanded (Figs. 6, 7A). Previous studies suggested that the shovel-shaped expansion of the snout seen in aetosaurus such as *Desmatosuchus smalli* (Fig. 7D; Small, 2002), *Stagonolepis robertsoni* (Fig. 7E; Walker, 1961), *Stagonolepis olenkae* (Sulej, 2010), and *Neo-aetosauroides engaeus* (Desojo and Báez, 2007) are associated with the use of digging (Desojo and Vizcaíno, 2009; Desojo et al., 2013). Our present understanding of aetosaurian phylogeny (Fig. 8) places aetosaurus with transversely expanded premaxillae into the Stagonolepidoidea, suggesting that this morphology is a synapomorphy for this group. *Tytophorax coccinarum* lacks this morphological character (i.e., shovel-shaped snout), as is the case for all aetosaurines with known cranial material (Fig. 8) including *Aetosaurus ferratus* (Fig. 7B; Schoch, 2007), *Stenomylti huangae* (Small and Martz, 2013), and *Paratytophorax andressorum* (Fig. 7C; Schoch and Desojo, 2016). Furthermore, the new cranial material of *Aetosauroides scagliai* (UFSM 11505; Biacchi Brust et al., 2018) bears an elongate external naris relative to the orbit, a non-tapering nasal, and a weakly developed anterior expansion of the premaxillae, demonstrating that these represent the plesiomorphic condition for Aetosauria (Fig. 8). A homodont dentition in *Aetosauroides scagliai* (Biacchi Brust et al., 2018), as well as a horizontal ventral jugal margin, provide further information on character distributions as both are also presently plesiomorphic for Aetosauria.

### CONCLUSIONS

The combination of character states present in the cranium of *Tytophorax coccinarum* clarifies some of the relationships and defining synapomorphies for some of the major clades within Aetosauria and Stagonolepidoidea. Combined with recent redescription and descriptions of the skulls of *Aetosaurus ferratus*, *Aetosauroides scagliai*, *Coahomasuchus chathamensis*,

*Neoaetosauroides engaeus*, *Paratytophorax andressorum*, *Stenomyti huangae*, *Stagonolepis olenkae*, and *Scutarx deltatylus* it is apparent that two major clades of stagonolepidids (i.e., the Stagonolepidoidea and the Aetosaurinae) possess different overall skull morphologies. The stagonolepidoids have more robust, elongate skulls, with laterally flared premaxillary tips, whereas the aetosaurines have proportionately shorter, more gracile skulls with tapered premaxillae. Although a robust morphology is yet to be described in the skull of *Revueltosaurus callenderi* (Parker et al., 2005; Marsh et al., 2020), the robust skull of *Aetosauroides scagliai* suggests that this is the plesiomorphic state and that the more gracile form is a synapomorphy of Aetosaurinae.

The heterodont dentition of *Tytophorax coccinarum* expands the range of dentition types for aetosaurians demonstrating diverse feeding strategies for the clade beyond the historical interpretation of them as strict herbivores (e.g., Walker, 1961) and supporting more recent hypotheses regarding omnivory and insectivory (Small, 2002; Desojo and Báez, 2007; Desojo and Vizcaíno, 2009; Desojo et al., 2013).

#### ACKNOWLEDGMENTS

Thank you to M. Fox, A. Gishlick, A. Behlke, W. Joyce, J. Gauthier, and the YPM crews for fieldwork, collection, preparation, curation, and transfer of the specimen. The specimen was collected from Petrified Forest National Park under research permit PEFO-2008-SCI-0012. Additional preparation was done by M. Smith (PEFO). The stratigraphic section is courtesy of J. Martz. Thanks to J. Payne for allowing us to scan PEFO 38001 at the Summit Healthcare Regional Medical Center. Thanks to J. Desojo and A. Heckert for constructive reviews. The opinions expressed herein are solely those of the authors and do not represent the views of the United States Government. This is Petrified Forest National Park paleontological contribution no. 69.

#### ORCID

William A. Reyes  <http://orcid.org/0000-0002-9967-2557>

William G. Parker  <http://orcid.org/0000-0002-6005-7098>

Adam D. Marsh  <http://orcid.org/0000-0002-3223-8940>

#### LITERATURE CITED

- Benton, M. J. 1983. The Triassic reptile *Hyperodapedon* from Elgin: functional morphology and relationships. *Philosophical Transactions of the Royal Society of London* 302:605–718.
- Biacchi Brust, A. C., J. B. Desojo, C. L. Schultz, V. D. Paes-Neto, and Á. A. S. Da-Rosa. 2018. Osteology of the first skull of *Aetosauroides scagliai* Casmiquela 1960 (Archosauria: Aetosauria) from the Upper Triassic of southern Brazil (*Hyperodapedon* Assemblage Zone) and its phylogenetic importance. *PLOS ONE* 13:e0201450.
- Cope, E. D. 1869. Synopsis of the extinct Batrachia, Reptilia, and Aves of North America. *Transactions of the American Philosophical Society* 14(1):1–252.
- Cope, E. D. 1875. Report on the geology of that part of northwestern New Mexico examined during the field-season of 1874; pp. 61–97 of separate issue, 981–1017 of full report in *Annual Report upon the Geographical Explorations West of the 100th Meridian [Wheeler Survey]*, Appendix LL. *Annual Report Chief of Engineers for 1875*.
- Cope, E. D. 1887. A contribution to the history of the vertebrata of the Trias of North America. *Proceedings of the American Philosophical Society* 24:209–228.
- Desojo, J. B., and A. M. Báez. 2007. Cranial morphology of the Late Triassic South American archosaur *Neoaetosauroides engaeus*: evidence for aetosaurian diversity. *Paleontology* 50:267–276.
- Desojo, J. B., and M. D. Ezcurra. 2011. A reappraisal of the taxonomic status of *Aetosauroides* (Archosauria, Aetosauria) specimens from the Late Triassic of South America and their proposed synonymy with *Stagonolepis*. *Journal of Vertebrate Paleontology* 31:596–609.
- Desojo, J. B., and S. F. Vizcaíno. 2009. Jaw biomechanics in the South American aetosaur *Neoaetosauroides engaeus*. *Paläontol Z* 83:499–510.
- Desojo, J. B., A. B. Heckert, J. W. Martz, W. G. Parker, R. S. Schoch, B. J. Small, and T. Sulej. 2013. Aetosauria: a clade of armoured pseudosuchians from the Upper Triassic continental beds. *Geological Society, London, Special Publications* 379:203–239.
- Drózdź, D. 2018. Osteology of a forelimb of an aetosaur *Stagonolepis olenkae* (Archosauria: Pseudosuchia: Aetosauria) from the Krasiejów locality in Poland and its probable adaptations for a scratch-digging behavior. *PeerJ* 6:e5595.
- Dubiel, R. F. 1989. Depositional and climatic setting of the Upper Triassic Chinle Formation, Colorado Plateau; pp. 171–187 in S. G. Lucas, A. P. Hunt (eds.), *Dawn of the age of dinosaurs in the American Southwest*. New Mexico Museum of Natural History, Albuquerque.
- Dubiel, R. F., J. T. Parrish, J. M. Parrish, and S. C. Good. 1991. The Pangaean Megamonsoon-Evidence from the Upper Triassic Chinle Formation, Colorado Plateau. *Palaios* 6:347–370.
- Fedorov, A., R. Beichel, J. Kalpathy-Cramer, J. Finet, J. C. Fillion-Robin, S. Pujol, C. Bauer, D. Jennings, F. Fennessy, M. Sonka, J. Buatti, S. Aylward, J. V. Miller, S. Pieper, and R. Kikinis. 2012. 3D Slicer as an image computing platform for the quantitative imaging network. *Magnetic Resonance Imaging* 30(9):1323–1341.
- Gauthier, J., and K. Padian. 1985. Phylogenetic, functional, and aerodynamic analyses of the origin of birds and their flight; pp. 185–197 in M. K. Hecht, J. H. Ostrom, G. Viohl, P. Wellnhofer (eds.), *The Beginning of Birds: Proceedings of the International Archaeopteryx Conference*. Freunde des Jura Museums, Eichstätt.
- George, I. D., and C. M. Holliday. 2013. Trigeminal nerve morphology in *Alligator mississippiensis* and its significance for crocodyliform facial sensation and evolution. *The Anatomical Record* 296:670–680.
- Goloboff, P. A., J. S. Farris, and K. C. Nixon. 2008. TNT, a free program for phylogenetic analysis. *Cladistics* 24:774–786.
- Heckert, A. B. 2002. A revision of the Upper Triassic Ornithischian Dinosaur *Revueltosaurus*, with a description of a new species. *New Mexico Museum of Natural History and Science Bulletin* 21:253–268.
- Heckert, A. B., and S. G. Lucas. 2000. Taxonomy, phylogeny, biostratigraphy, biochronology, paleobiogeography, and evolution of the Late Triassic Aetosauria (Archosauria: Crurotarsi). *Zentralblatt für Geologie und Paläontologie, Teil I, Heft 11–12*:1539–1587.
- Heckert, A. B., N. C. Fraser, and V. P. Schneider. 2017. A new species of *Coahomasuchus* (Archosauria, Aetosauria) from the Upper Triassic Pekin Formation, Deep River Basin, North Carolina. *Journal of Paleontology* 91:162–178.
- Heckert, A. B., S. G. Lucas, L. F. Rinehart, M. D. Celleskey, J. A. Spielmann, and A. P. Hunt. 2010. Articulated skeletons of the aetosaur *Tytophorax coccinarum* Cope (Archosauria: Stagonolepididae) from the Upper Triassic Bull Canyon Formation (Revueltian: early-mid Norian), eastern New Mexico, USA. *Journal of Vertebrate Paleontology* 30:619–642.
- Hildebrand, M. 1974. *Analysis of Vertebrate Structure*. John Wiley & Sons, New York, New York, 710 pp.
- Hoffman, D. K., A. B. Heckert, and L. E. Zanno. 2018. Under the armor: X-ray computed tomographic reconstruction of the internal skeleton of *Coahomasuchus chathamensis* (Archosauria: Aetosauria) from the Upper Triassic of North Carolina, USA, and a phylogenetic analysis of Aetosauria. *PeerJ* 6:e4368.
- Huene, F. v. 1915. On reptiles of the New Mexico Triassic in the Cope collection. *Bulletin of the American Museum of Natural History* 34:485–507.
- Hunt, A. P., S. G. Lucas, and P. K. Reser. 1993. A complete skeleton of the stagonolepidid *Tytophorax coccinarum* from the Upper Triassic Bull Canyon Formation of east-central New Mexico, USA. *New Mexico Museum of Natural History and Science Bulletin* 3:209–212.
- Irmis, R. B., R. Mundil, J. W. Martz, and W. G. Parker. 2011. High-resolution U–Pb ages from the Upper Triassic Chinle Formation (New Mexico, USA) support a diachronous rise of dinosaurs. *Earth and Planetary Science Letters* 309:258–267.
- Kent, D. V., and L. Tauxe. 2005. Corrected Late Triassic latitudes for continents adjacent to the North Atlantic. *Science* 307:240–244.

- Kent, D. V., P. E. Olsen, C. Rasmussen, C. Lepre, R. Mundil, R. B. Irmis, G. E. Gehrels, D. Giesler, J. W. Geissman, and W. G. Parker. 2018. Empirical evidence for stability of the 405-kiloyear Jupiter–Venus eccentricity cycle over hundreds of millions of years. *Proceedings of the National Academy of Sciences* 115:6153–6158.
- Kent, D. V., P. E. Olsen, C. Lepre, C. Rasmussen, R. Mundil, G. E. Gehrels, D. Giesler, R. B. Irmis, J. W. Geissman, and W. G. Parker. 2019. Magnetostratigraphy of the entire Chinle Formation (Norian Age) in a scientific drill core from Petrified Forest National Park (Arizona, USA) and implications for regional and global correlations in the Late Triassic. *Geochemistry, Geophysics, Geosystems* 10.1029/2019GC008474.
- Kirby, R. E. 1991. A vertebrate fauna from the Upper Triassic Owl Rock Member of the Chinle Formation of northern Arizona. M.Sc. thesis, Northern Arizona University, Flagstaff, Arizona, 476 pp.
- Kirby, R. E. 1993. Relationships of Late Triassic basin evolution and faunal replacement events in the southwestern United States: perspectives from the upper part of the Chinle Formation in northern Arizona. *New Mexico Museum of Natural History and Science Bulletin* 3:232–242.
- Long, R. A. and K. L. Ballew. 1985. Aetosaur dermal armour from the Late Triassic of southwestern United States: perspectives from the upper part of the Chinle Formation of Petrified Forest National Park. *Museum of Northern Arizona Bulletin* 54:45–68.
- Long, R. A., and P. A. Murry. 1995. Late Triassic (Carnian and Norian) tetrapods from the Southwestern United States. *New Mexico Museum of Natural History and Science Bulletin* 4:99–108.
- Marsh, O. C. 1884. The classification and affinities of dinosaurian reptiles. *Nature* 31:68–69.
- Marsh, A. D., M. E. Smith, W. G. Parker, R. B. Irmis, and B. T. Kligman. 2020. Skeletal anatomy of *Acaenasuchus geoffreyi* Long and Murry, 1995 (Archosauria: Pseudosuchia) and its implications for the origin of the aetosaurian carapace. *Journal of Vertebrate Paleontology* 40: e1794885.
- Martz, J. W. 2002. The morphology and ontogeny of *Typhothorax coccinarum* (Archosauria, Stagonolepididae) from the Upper Triassic of the American Southwest. M.S. thesis, Department of Geoscience, Texas Tech University, Lubbock, Texas, 279 pp.
- Martz, J. W., and W. G. Parker. 2017. Revised formulation of the Late Triassic land vertebrate “faunachrons” of Western North America: Recommendations of codifying nascent systems of vertebrate biochronology; pp. 39–125 in W. G. Parker, K. E. Zeigler (eds.) *Terrestrial Depositional Systems: Deciphering Complexities Through Multiple Stratigraphic Methods*. Amsterdam, Elsevier.
- Martz, J. W., and B. J. Small. 2006. *Tecovasuchus chatterjeei*, a new aetosaur (Archosauria: Stagonolepididae) from the Tecovas Formation (Carnian, Upper Triassic) of Texas. *Journal of Vertebrate Paleontology* 26(2):308–320.
- Martz, J. W., W. G. Parker, L. Skinner, J. J. Raucchi, P. Umhoefer, and R. C. Blakey. 2012. Geologic Map of Petrified Forest National Park, Arizona. Arizona Geological Survey Contributed Map CR-12-A, 1 map sheet, 1:50,000 map scale, 18p.
- Martz, J. W., B. Mueller, S. J. Nesbitt, M. R. Stocker, W. G. Parker, M. Atanassov, N. Fraser, J. Weinbaum, and J. R. Lehane. 2013. A taxonomic and biostratigraphic re-evaluation of the Post Quarry vertebrate assemblage from the Cooper Canyon Formation (Dockum Group, Upper Triassic) of southern Garza County, western Texas. *Earth and Environmental Science Transactions of the Royal Society of Edinburgh* 103:339–364.
- Nesbitt, S. J., and M. R. Stocker. 2008. The vertebrate assemblages of the Late Triassic Canjilon quarry (Northern New Mexico, USA), and the importance of apomorphy-based assemblage comparisons. *Journal of Vertebrate Paleontology* 28:1063–1072.
- Nordt, L., S. Atchley, and S. Dworkin. 2015. Collapse of the Late Triassic Megamonsoon in western equatorial Pangea, present-day American Southwest. *Geological Society of America Bulletin* 127 (11–12):1798–1815.
- Parker, W. G. 2005a. A new species of the Late Triassic aetosaur *Desmatosuchus* (Archosauria: Pseudosuchia). *Comptes Rendus Palevol* 4:327–340.
- Parker, W. G. 2005b. Faunal review of the Upper Triassic Chinle Formation of Arizona. *Mesa Southwest Museum Bulletin* 11:34–54.
- Parker, W. G. 2007. Reassessment of the Aetosaur ‘*Desmatosuchus chamaensis*’ with a reanalysis of the phylogeny of the Aetosauria (Archosauria: Pseudosuchia). *Journal of Systematic Palaeontology* 5:41–68.
- Parker, W. G. 2008. Description of new material of the aetosaur *Desmatosuchus spurensis* (Archosauria: Suchia) from the Chinle Formation of Arizona and a revision of the genus *Desmatosuchus*. *PaleoBios* 28:1–40.
- Parker, W. G. 2013. Redescription and taxonomic status of specimens of *Episcoposaurus* and *Typhothorax*, the earliest known aetosaurs (Archosauria: Suchia) from the Upper Triassic of western North America, and the problem of proxy “holotypes”. *Earth and Environmental Science Transactions of the Royal Society of Edinburgh* 103:313–338.
- Parker, W. G. 2016a. Revised phylogenetic analysis of the Aetosauria (Archosauria: Pseudosuchia): Assessing the effects of incongruent morphological character sets. *PeerJ* 4:e1583.
- Parker, W. G. 2016b. Osteology of the Late Triassic aetosaur *Scutarx deltatylus* (Archosauria: Pseudosuchia). *PeerJ* 4:e2411.
- Parker, W. G. 2018. Redescription of *Calyptosuchus (Stagonolepis) wellsi* (Archosauria: Pseudosuchia: Aetosauria) from the Late Triassic of the Southwestern United States with a discussion of genera in vertebrate paleontology. *PeerJ* 6:e4291.
- Parker, W. G., and J. W. Martz. 2011. The Late Triassic (Norian) Adamanian–Revueletian tetrapod faunal transition in the Chinle Formation of Petrified Forest National Park, Arizona. *Earth and Environmental Science Transactions of the Royal Society of Edinburgh* 101:231–260.
- Parker, W. G., R. B. Irmis, S. J. Nesbitt, J. W. Martz, and L. S. Browne. 2005. The Late Triassic pseudosuchian *Revueletosaurus callenderi* and its implications for the diversity of early ornithischian dinosaurs. *Proceedings of the Royal Society* 272:963–969.
- Parrish, J. M. 1994. Cranial osteology of *Longosuchus meadei* and the phylogeny and distribution of the Aetosauria. *Journal of Vertebrate Paleontology* 14:196–209.
- Ramezani, J., G. D. Hoke, D. E. Fastovsky, S. A. Bowring, F. Therrien, S. I. Dworkin, S. C. Atchley, and L. C. Nordt. 2011. High precision U–Pb zircon geochronology of the Late Triassic Chinle Formation, Petrified Forest National Park (Arizona, USA): Temporal constraints on the early evolution of dinosaurs. *Geological Society of America* 123:2142–2159.
- Roberto-Da-Silva, L., J. B. Desojo, S. F. Cabreira, A. S. S. Aires, R. T. Müller, C. P. Pacheco, and S. Dias-Da-Silva. 2014. A new aetosaur from the Upper Triassic of the Santa Maria Formation, southern Brazil. *Zootaxa* 3764:240–278.
- Sawin, H. J. 1947. The pseudosuchian reptile *Typhothorax meadei*. *Journal of Paleontology* 21(3):201–238.
- Schoch, R. R. 2007. Osteology of the small archosaur *Aetosaurus* from the Upper Triassic of Germany. *Neues Jahrbuch für Geologie und Paläontologie Abhandlungen* 246(1):1–35.
- Schoch, R. R., and J. B. Desojo. 2016. Cranial anatomy of the aetosaur *Paratyphothorax andressorum*. *Neues Jahrbuch für Geologie und Paläontologie Abhandlungen* 279:73–95.
- Small, B. 2002. Cranial anatomy of *Desmatosuchus haplocerus* (Reptilia: Archosauria: Stagonolepididae). *Zoological Journal of the Linnean Society* 136:97–111.
- Small, B., and J. W. Martz. 2013. A new aetosaur from the Upper Triassic Chinle Formation of the Eagle Basin, Colorado, USA. *Geological Society, London, Special Publications* 379:393–412.
- Spielmann, J. A., S. G. Lucas, and A. B. Heckert. 2007. Tetrapod fauna of the Upper Triassic (Revueletian) Owl Rock Formation, Chinle Group, Arizona. *New Mexico Museum of Natural History and Science Bulletin* 41:371–383.
- Sulej, T. 2010. The skull of an early Late Triassic aetosaur and the evolution of the stagonolepidid archosaurian reptiles. *Zoological Journal of the Linnean Society* 158:860–861.
- Walker, A. D. 1961. Triassic reptiles from the Elgin area: *Stagonolepis*, *Dasygnathus* and their allies. *Philosophical Transactions of the Royal Society B* 244:103–204.
- Zittel, K. A. 1887–1890. *Handbuch der Palaeontologie*. 1. Abteilung: Palaeozoologie. 3. Oldenbourg, München & Leipzig.

Submitted December 23, 2019; revisions received August 23, 2020; accepted September 17, 2020.

Handling Editor: Elizabeth Martin-Silverstone